Rheodielectric Behavior of Entangled *cis*-Polyisoprene under Fast Shear

H. Watanabe,* S. Ishida, and Y. Matsumiya

Institute for Chemical Research, Kyoto University, Uji, Kyoto 611-0011, Japan

Received April 9, 2002

ABSTRACT: For entangled solutions of linear and star-branched *cis*-polyisoprene (PI) chains, rheodielectric tests were conducted to examine the nonequilibrium chain dynamics under steady shear. The PI chains had the type-A dipoles parallel along their backbone, and the observed rheodielectric behavior reflected the dynamics (fluctuation) of the end-to-end vector of the linear chain and/or the star arm in the shear gradient direction. This behavior changed only slightly, in both relaxation time and intensity, with the shear rate $\dot{\gamma}$ even in the significantly thinning regime at $1/\tau_1 < \dot{\gamma} < 1/\tau_{\text{Rouse}}$, with τ_1 = terminal relaxation time and τ_{Rouse} = Rouse relaxation time for the chain length equilibration. Comparison of the $\dot{\gamma}$-insensitive rheodielectric intensity data and the non-Newtonian viscosity/normal stress data indicated that an isochronal orientational cross-correlation emerged over some number (β) of entanglement segments under fast shear. This result was analyzed on the basis of the molecular picture of dynamic tube dilation (DTD) induced by the convective constraint release (CCR). The analysis suggested $\beta \cong 1.8$ and $\cong 1.2$ for the linear and star chains at the largest $\dot{\gamma}$ examined. The CCR−DTD picture was consistent also with the observed $\dot{\gamma}$-insensitivity of the rheodielectric relaxation time. Furthermore, the current CCR models for the linear chain were examined for the rheodielectric data. It turned out that the observed $\dot{\gamma}$-insensitivity of the relaxation time was not straightforwardly deduced from the models.

1. Introduction

Entangled polymer chains exhibit significant nonlinearities in their viscoelastic properties under fast flow/large strain.[1−3] For example, the steady-state shear viscosity $\eta(\dot{\gamma})$ under fast flow decreases with increasing shear rate $\dot{\gamma}$, and this decrease is described by a power law $\eta \propto \dot{\gamma}^{-\delta}$ ($\delta \cong 0.8$) in a considerably wide rage of $\dot{\gamma}$ irrespective of the entanglement density of the chains.[1,2] Molecular description of such nonlinear behavior has been one of the central subjects of polymer physics.[2−4] In particular, efforts[4−10] have been made to describe the nonlinear viscoelasticity with the tube model in which the entanglement is represented as a tube surrounding the chain.

In the early version of the model assuming the fixed and unleakable tube,[4] the tube and chain therein are strongly orientated under fast shear. This strong orientation results in a very strong decrease of η ($\propto \dot{\gamma}^{-1.5}$) contradicting the observation.[4] This problem cannot be removed even if the chain stretching mechanism[5,6] is incorporated in the model. Thus, the recent tube model incorporates the *convective constraint release* (*CCR*) mechanism[8−10] explained below.

At shear rates $\dot{\gamma}$ larger than the terminal relaxation frequency $1/\tau_1$ but smaller than the Rouse frequency $1/\tau_{\text{Rouse}}$ for equilibration of the contour length of the (primitive) chain, the chain is orientated but not stretched on average. Under the shear flow at those $\dot{\gamma}$, the chain transiently stretched by the flow shrinks to recover its equilibrium (unstretched) contour length L_{eq}. This shrinkage of the chain releases the topological constraint for a surrounding entangled chain, thereby allowing the lateral leakage of the latter chain from its own tube to weaken its orientation. With this CCR mechanism first proposed by Ianniruberto and Marrucci (IM)[8] and later combined with the other mechanisms by Mead, Larson, and Doi (MLD)[9] and by Milner, McLeish, and Likhtman (MML),[10] the problem of the early model (the strong decrease of η with increasing $\dot{\gamma}$) can be successfully removed. In particular, the MLD and MML models reproduce the viscosity and first normal stress difference data with a considerable accuracy.

Thus, the current tube model incorporating the CCR and other mechanisms such as the thermal constraint release (TCR) and contour length fluctuation (CLF) successfully describes the nonlinear viscoelastic properties. However, we have to remember that the viscoelastic properties of the chain reflect a particular average of the chain conformation, i.e., the isochronal orientational anisotropy of individual entanglement segments.[3] In other words, the agreement of the CCR model prediction and the viscoelastic data does not necessarily indicate that the chain motion considered in the model coincides with the actual nonequilibrium motion under flow. From this point of view, it is highly desirable to examine not only the viscoelastic properties but also the other properties that differently average the same motion/conformation of the chain.

The dielectric property of the so-called type-A chains[11] having the dipoles parallel along the chain backbone serves for this purpose. This property reflects the orientational correlation of two segments *at two separate times* (e.g., 0 and t).[12−17] Thus, the chain conformation and motion are differently averaged in the viscoelastic and dielectric properties. This difference can be utilized to examine detailed features of the chain dynamics: For example, recent studies[12−17] compared the linear viscoelastic and dielectric data of type-A *cis*-polyisoprene (PI) chains to reveal that the molecular picture of the dynamic tube dilation (DTD) at equilibrium, incorporated in the tube model,[18−20] is valid for the terminal relaxation of linear chains but not for the star-branched chains.

Considering this usefulness of the dielectric property, we have examined the rheodielectric behavior of entangled linear and star PI chains under steady shear.

* To whom correspondence should be addressed.

10.1021/ma020562y CCC: $22.00
Published on Web 10/08/2002

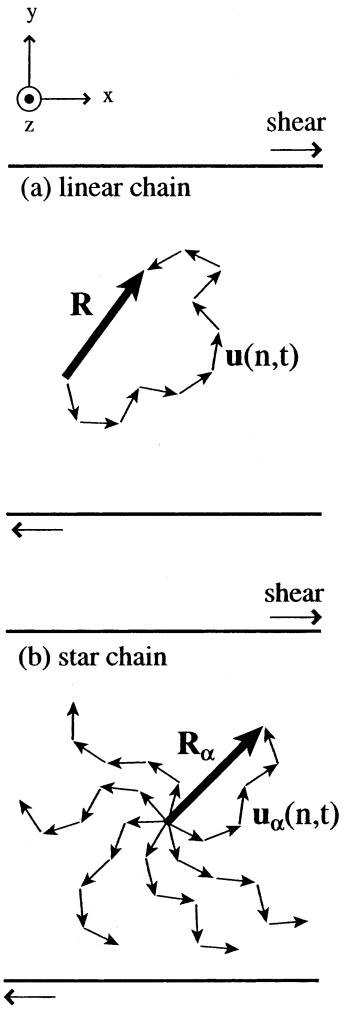

Figure 1. Schematic illustration of type-A linear and star chains under steady shear. Thin arrows indicate the bond vectors **u** of the entanglement segments (having the dipoles parallel to **u**).

This behavior, reflecting the chain motion/conformation in the shear gradient direction, changed with $\dot\gamma$ only slightly even in the significantly thinning regime at $1/\tau_1 < \dot\gamma < 1/\tau_{\text{Rouse}}$. Comparison of the rheodielectric intensity and the nonlinear viscoelastic data indicated that an isochronal orientational cross-correlation emerged over some number (β) of successive entanglement segments under fast shear.

Furthermore, we analyzed those rheodielectric and viscoelastic data on the basis of the molecular picture of the CCR-induced DTD: The segments were considered to be mutually equilibrated through this CCR−DTD mechanism to exhibit the isochronal cross-correlation. This analyses gave the number $\beta \cong 1.8$ and 1.2 for the linear and star chains at the largest $\dot\gamma$ examined. We also discussed the weak $\dot\gamma$ dependence of the rheodielectric relaxation time of the linear and star chains in relation to the CCR−DTD mechanism.

In this paper, we present these results together with a result of brief comparison of the current CCR models[8−10] and the rheodielectric data.

2. Theoretical Section

2.1. Molecular Expression of Viscoelastic and Dielectric Properties. We consider the entangled, monodisperse type-A linear and star chains schematically shown in Figure 1. The linear chain is composed of N entanglement segments, and the star chain is composed of q arms each having N_a entanglement segments. Thin arrows indicate the bond vectors of these segments at a time t, $\mathbf{u}(n,t)$ and/or $\mathbf{u}_\alpha(n,t)$ with n being the segment index. The thick arrows denote the end-to-end vectors of the linear chain and/or star arm, $\mathbf{R}(t)$ and/or $\mathbf{R}_\alpha(t)$. Hereafter, the arm index α for the star chain is explicitly shown only when necessary.

The linear and star chains are subjected to the steady shear. The shear, shear-gradient, and vorticity directions are defined as the x, y, and z directions, respectively. The shear rate $\dot\gamma$ examined in this paper is lower than the Rouse frequency for the chain length equilibration, $1/\tau_{\text{Rouse}}$. Under this condition, we may safely assume that the entanglement segments have the equilibrium size, a ($=\langle \mathbf{u}^2\rangle_{\text{eq}}^{1/2}$). Correspondingly, the *primitive* chain[4] defined as a sequence of the axes of the connected entanglement segments is not stretched. Hereafter, the primitive chain is simply referred to as the "chain" unless a confusion arises.

Thus, under the shear examined, the primitive chain has the equilibrium contour length,[4−6,8−10] $L_{\text{eq}} = Na$ and $N_a a$ for the linear chain and star arm. For this case, the chain conformation and dynamics are fully specified by a set of unit bond vectors, $\tilde{\mathbf{u}}(n,t) = \mathbf{u}(n,t)/a$. The viscoelastic and dielectric properties are determined by the chain conformation/dynamics and expressed in terms of $\tilde{\mathbf{u}}$. These expressions are summarized below. For simplicity of the expressions, the segment number per chain is hereafter denoted by N_{chain} ($=N$ and qN_a for the linear and star chains), and the summation $\sum_{\text{all } n}^{N_{\text{chain}}} \cdots$ represents $\sum_{n=1}^{N} \cdots$ for the linear chain and $\sum_{n=1}^{N_a}\sum_{\alpha=1}^{q} \cdots$ for the star chain.

2.1.1. Viscoelastic Properties. The stress of the *unstretched* primitive chains reflects the isochronal orientational anisotropy of individual entanglement segments.[3,4] For these chains, the deviatoric part of the stress tensor $\boldsymbol{\sigma}$ is expressed in terms of the dyadic of **u** and/or $\tilde{\mathbf{u}}$,[3,4]

$$\boldsymbol{\sigma} = \frac{3\nu N_{\text{chain}} f k_B T}{a^2}\left\{\langle \mathbf{u}\mathbf{u}\rangle - \langle \mathbf{u}^2\rangle\frac{\mathbf{I}}{3}\right\} = 3G_N\left\{\langle \tilde{\mathbf{u}}\tilde{\mathbf{u}}\rangle - \frac{\mathbf{I}}{3}\right\} \quad (1)$$

Here, ν is the number density of the chain, k_B is the Boltzmann constant, T is the absolute temperature, **I** is the unit tensor, f is a numerical factor ($f = 1$ for the affine deformation considered in the rubber elasticity theory and $f = 4/5$ in the Doi−Edwards theory),[3,4] and G_N ($=\nu N_{\text{chain}} f k_B T$) is the entanglement plateau modulus. The $\langle \tilde{\mathbf{u}}\tilde{\mathbf{u}}\rangle$ appearing in eq 1 represents the average

$$\langle \tilde{\mathbf{u}}\tilde{\mathbf{u}}\rangle = \frac{1}{N_{\text{chain}}}\sum_{\text{all } n}^{N_{\text{chain}}} \langle \tilde{\mathbf{u}}(n,t)\tilde{\mathbf{u}}(n,t)\rangle \quad \text{for linear/star chains} \quad (2)$$

Hereafter, the averages shown without the segment index n (such as $\langle \tilde{\mathbf{u}}\tilde{\mathbf{u}}\rangle$) represent the averages taken for all entanglement segments.

From eqs 1 and 2, the viscosity η and the normal stress coefficients Ψ_1 and Ψ_2 under steady shear are related to the second-moment averages of the components of $\tilde{\mathbf{u}}$

$$\eta = \frac{3G_N}{\dot{\gamma}}\langle \tilde{u}_x \tilde{u}_y \rangle \tag{3}$$

$$\Psi_1 = \frac{3G_N}{\dot{\gamma}^2}\{\langle \tilde{u}_x{}^2 \rangle - \langle \tilde{u}_y{}^2 \rangle\} \tag{4}$$

$$\Psi_2 = \frac{3G_N}{\dot{\gamma}^2}\{\langle \tilde{u}_x{}^2 \rangle + 2\langle \tilde{u}_y{}^2 \rangle - 1\} \tag{5}$$

(In eq 5, we have utilized a relationship $\langle \tilde{u}_x{}^2 \rangle + \langle \tilde{u}_y{}^2 \rangle + \langle \tilde{u}_z{}^2 \rangle = 1$ to express Ψ_2 in terms of $\langle \tilde{u}_x{}^2 \rangle$ and $\langle \tilde{u}_y{}^2 \rangle$.) Thus, the second-moment averages can be evaluated from the viscoelastic data.

2.1.2. Dielectric Properties. If a system is stationary against time and the local equilibrium is achieved, e.g., either in the quiescent equilibrium state or under steady shear, the dielectric relaxation function $\Theta(t)$ is given by the autocorrelation of the component of the polarization $P_E(t)$ in the direction of the applied electric field:[21−23]

$$\Theta(t) = \langle P_E(t+t_r)P_E(t_r)\rangle = \Delta\epsilon\ \Phi(t) \quad (t \geq 0) \tag{6}$$

Here, $\Delta\epsilon$ ($=\langle [P_E(t_r)]^2 \rangle$) is the dielectric intensity, $\Phi(t)$ ($=\langle P_E(t+t_r)P_E(t_r)\rangle / \langle [P_E(t_r)]^2 \rangle$) is the normalized dielectric relaxation function ($\Phi(0) = 1$), and t_r is a reference time arbitrarily chosen in the stationary state. (The $\Delta\epsilon$ and $\Phi(t)$ are not dependent on t_r, and t_r is often chosen to be zero.) In our rheodielectric set up, the electric field is applied in the y direction (shear-gradient direction) and the autocorrelation of the y component of the polarization P_y is detected.

The type-A linear and star chains have the dipoles parallel to **u**. Thus, the polarization **P** of the linear chain is proportional to its end-to-end vector, **R**, while **P** of the star chain is proportional to a sum of the end-to-end vectors of the arms, $\Sigma_\alpha \mathbf{R}_\alpha$. For these chains, the $\Delta\epsilon$ and $\Phi(t)$ detected in the y direction are expressed in terms of the y component of $\tilde{\mathbf{u}}$ of the entanglement segments:[24]

$$\Delta\epsilon = K_\epsilon \nu a^2 Q \quad \text{with } Q = \sum_{\text{all } n}^{N_{\text{chain}}} \sum_{\text{all } n'}^{N_{\text{chain}}} \langle \tilde{u}_y(n,t_r)\tilde{u}_y(n',t_r)\rangle \tag{7}$$

and

$$\Phi(t) = \frac{1}{Q}\sum_{\text{all } n}^{N_{\text{chain}}} \sum_{\text{all } n'}^{N_{\text{chain}}} \langle \tilde{u}_y(n,t+t_r)\tilde{u}_y(n',t_r)\rangle \tag{8}$$

In eq 7, ν represents the number density of the chains, and K_ϵ is a constant independent of N, N_a, q, and $\dot{\gamma}$. (K_ϵ is determined by the magnitude of the type-A dipoles.[15,21,22].)

The time-dependent part of the rheodielectric relaxation, reflecting the fluctuation of R_y under the shear, is described by $\Phi(t)$ (eq 8). This $\Phi(t)$ is contributed from the autocorrelation $\langle \tilde{u}_y(n,t+t_r)\tilde{u}_y(n,t_r)\rangle$ and the cross-correlation $\langle \tilde{u}_y(n,t+t_r)\tilde{u}_y(n',t_r)\rangle_{n'\neq n}$ in individual chains.[24] The contribution of the cross-correlation is an intrinsic feature of the dielectric relaxation of type-A chains. Concerning this point, we should again emphasize that the same motion/conformation of the chain is differently averaged in the dielectric and viscoelastic properties, the latter detecting only isochronal orientational anisotropy (isochronal autocorrelation; cf. eq 1).

The isochronal cross-correlation $\langle \tilde{u}_y(n,t_r)\tilde{u}_y(n',t_r)\rangle_{n'\neq n}$ is included in the expression of $\Delta\epsilon$ (eq 7). This cross-correlation vanishes in the quiescent equilibrium state where the chain has the isotropic Gaussian conformation. However, under the fast shear examined in this study, the chain is shear-oriented and the isochronal cross-correlation may emerge over a sequence of entanglement segments (because of the CCR mechanism). Considering this situation, we introduce a number, β, of the segments exhibiting the isochronal cross-correlation: This cross-correlation should decay with increasing contour distance between the segments, and β is regarded as a *cutoff distance*.

Utilizing this β, we can rewrite eq 7 as

$$\Delta\epsilon(\dot{\gamma}) = K_\epsilon\, \nu N_{\text{chain}} a^2 \{\langle \tilde{u}_y{}^2 \rangle + (\beta - 1)\langle \tilde{u}_y \tilde{u}_y' \rangle\} \quad \text{for linear/star chains under shear} \tag{9}$$

with

$$\langle \tilde{u}_y{}^2 \rangle = \frac{1}{N_{\text{chain}}}\sum_{\text{all } n}^{N_{\text{chain}}} \langle [\tilde{u}_y(n,t_r)]^2 \rangle \tag{10}$$

and

$$\langle \tilde{u}_y \tilde{u}_y' \rangle = \frac{1}{N_{\text{chain}}(\beta - 1)}\sum_{\text{all } n}^{N_{\text{chain}}(\beta\text{-}1)} \sum_{n'\neq n}^{} \langle [\tilde{u}_y(n,t_r)\tilde{u}_y(n',t_r)]\rangle \tag{11}$$

In eq 11, the summation $\sum_{n'\neq n}^{(\beta-1)}$ is taken for the $\beta - 1$ segments (indexed with n') correlated with a given segment (indexed with n). Namely, eq 11 gives the magnitude of the shear-induced cross-correlation in the sequence of the β segments.

In the quiescent equilibrium state, the chain is in the Gaussian state to have $\langle \tilde{u}_y{}^2 \rangle_{eq} = {}^1/_3$ and $\beta = 1$ (no isochronal cross-correlation). The corresponding zero-shear dielectric intensity is given by $\Delta\epsilon(0) = K_\epsilon \nu N_{\text{chain}} a^2/3$ (cf. eq 9). Normalizing the $\Delta\epsilon(\dot{\gamma})$ (eq 9) by this $\Delta\epsilon(0)$, we find

$$\frac{\Delta\epsilon(\dot{\gamma})}{\Delta\epsilon(0)} = 3\{\langle \tilde{u}_y{}^2 \rangle + (\beta\text{-}1)\langle \tilde{u}_y \tilde{u}_y' \rangle\} \tag{12}$$

The average $\langle \tilde{u}_y{}^2 \rangle$ can be evaluated from the viscoelastic data; see eqs 4 and 5. Thus, a comparison of the $\langle \tilde{u}_y{}^2 \rangle$ and $\Delta\epsilon(\dot{\gamma})/\Delta\epsilon(0)$ data enables us to determine the cross-correlation term, $(\beta - 1)\langle \tilde{u}_y \tilde{u}_y' \rangle$.

2.2. Expression of ϵ^*. In this paper, we present the dynamic dielectric constant ϵ' and dielectric loss ϵ'' that are given by the Fourier transformation of the dielectric relaxation function[15,22] and obey a phenomenological framework similar to that for the viscoelastic moduli G' and G''. This framework, utilized in our later analysis of the rheodielectric data, is summarized below.

The normalized dielectric relaxation function $\Phi(t)$ (cf. eq 8) is expressed in terms of the relaxation time τ_p ($\tau_1 > \tau_2 > \tau_3$ ...) and normalized intensity g_p of the pth dielectric mode, $\Phi(t) = \Sigma_{p\geq 1}\, g_p \exp[-t/\tau_p]$ (with $\Sigma_{p\geq 1}\, g_p = 1$).[12,13,15] ϵ' and ϵ'' are conveniently expressed in terms of this dielectric spectrum $\{g_p,\tau_p\}$ as[12,13,15]

$$\epsilon_0 - \epsilon'(\omega) = \Delta\epsilon \sum_{p\geq 1} g_p \frac{\omega^2 {\tau_p}^2}{1+\omega^2 {\tau_p}^2},$$

$$\epsilon''(\omega) = \Delta\epsilon \sum_{p\geq 1} g_p \frac{\omega\tau_p}{1+\omega^2 {\tau_p}^2} \quad (13)$$

where ϵ_0 is the static dielectric constant and $\Delta\epsilon$ is the dielectric intensity.

As noted from eq 13, the ω dependence of the $\epsilon_0 - \epsilon'$ and ϵ'' data reflects the dielectric mode distribution, and an integral of ϵ'' gives the dielectric intensity,

$$\Delta\epsilon = \frac{2}{\pi}\int_{-\infty}^{\infty} \epsilon'' \, \mathrm{d}(\ln\omega) = \frac{2}{\pi}\int_0^{\infty} \frac{\epsilon''}{\omega}\, \mathrm{d}\omega \quad (14)$$

For the dielectric relaxation due to the global motion of the PI chain, this integral is conducted for the ϵ'' data reflecting only this motion (not contributed from the local/fast motion of individual monomeric segments). The $\Delta\epsilon$ thus obtained is related to the chain conformation through eq 9.

Equation 13, being analogous to the expression of G' and G'' in terms of the viscoelastic spectrum, indicates that $\epsilon_0 - \epsilon'$ and ϵ'' exhibit the terminal tails, $\epsilon_0 - \epsilon' \propto \omega^2$ and $\epsilon'' \propto \omega$ at low ω ($<1/\tau_1$). From these tails, we can define the second-moment average dielectric relaxation time:[12,15]

$$\langle\tau_\epsilon\rangle_w = \frac{[\{\epsilon_0 - \epsilon'(\omega)\}/\omega^2]_{\omega\to 0}}{[\epsilon''(\omega)/\omega]_{\omega\to 0}} = \frac{\sum_{p\geq 1} g_p {\tau_p}^2}{\sum_{p\geq 1} g_p \tau_p} \quad (15)$$

This $\langle\tau_\epsilon\rangle_w$ can be utilized as the *terminal* dielectric relaxation time.[15] (Note that $\langle\tau_\epsilon\rangle_w$ is analogous to the terminal viscoelastic relaxation time[2,3] $\langle\tau_G\rangle_w$ given as a product of the zero-shear viscosity η_0 and the steady-state compliance ${J_e}^0$.)

From eq 13, we can also define a quantity analogous to ${J_e}^0$:

$$\vartheta_\epsilon = \left[\frac{\epsilon_0 - \epsilon'(\omega)}{\{\epsilon''(\omega)\}^2}\right]_{\omega\to 0} = \frac{1}{\Delta\epsilon}\frac{\sum_{p\geq 1} g_p {\tau_p}^2}{[\sum_{p\geq 1} g_p \tau_p]^2} \quad (16)$$

This ϑ_ϵ, hereafter referred to as the "dielectric compliance", gives a reciprocal of the dielectric intensity tuned with the slow dielectric mode distribution. We can utilize ${\vartheta_\epsilon}^{-1}$ as a measure of the terminal dielectric intensity (in analogy to the use of $1/{J_e}^0$ as the terminal viscoelastic intensity).

The width of the dielectric mode distribution can be represented by a product, $\vartheta_\epsilon\Delta\epsilon = [\Sigma_{p\geq 1} g_p {\tau_p}^2]/[\Sigma_{p\geq 1} g_p \tau_p]^2$. The $\Delta\epsilon$ is analogous to the plateau modulus G_N, and the product $\vartheta_\epsilon\Delta\epsilon$ corresponds to the well-known measure of the viscoelastic mode distribution,[1-3] ${J_e}^0 G_N$.

3. Experimental Section

3.1. Materials. Linear and six-arm star *cis*-polyisoprene (PI) samples with narrow molecular weight distribution were utilized for the rheodielectric and viscoelastic tests. The linear PI sample was purchased from Polymer Source Inc. and fractionated once from benzene/methanol mixture to remove a contaminated high-M component.

Table 1. Characteristics of PI Samples

code	$10^{-3}M_w$ [a]	$10^{-3}M_a$ [a,b]	M_w/M_n [a]
	Linear PI		
I-1190	1190		1.11
	Six-Arm Star PI		
6(I-179)	1070	179	1.03

[a] Determined from RI and LALS signals. [b] Arm molecular weight.

The star PI sample was anionically synthesized in high vacuum at room temperature. *sec*-Butyllithium and heptane were utilized as the initiator and solvent, respectively. In the synthesis, an aliquot of the linear PI anions was recovered for the characterization of the star arm, and the remaining anions were allowed to react with a hexafunctional coupler, bis-(trichloromethyl silyl)ethane. The concentration of this coupler was set to be ~80% equimolar to the anions to ensure the full coupling. The crude product of the coupling reaction was fractionated from benzene/methanol mixtures for 20 times to thoroughly remove the excess (unreacted) arms and recover the monodisperse six-arm star PI samples.

The star and linear PI samples were characterized with GPC (CO-8020 and DP-8020, Tosoh) having a refractive index increment (RI) monitor combined with a law-angle laser-light scattering (LALS) photometer (LS-8000, Tosoh). The eluent was THF, and monodisperse linear PI samples[12,13,25] were utilized as the RI/LALS signal standards. The molecular weight and polydispersity of these samples determined from the RI/LALS signals are summarized in Table 1. The sample code number denotes $10^{-3}M$ of the linear chain and/or $10^{-3}M_a$ of the star arm.

The PI star arms had the type-A dipoles parallel along the arm backbone, and these dipoles were once inverted at the branching point. The linear PI chains had the noninverted type-A dipoles. These linear/star samples were freeze-dried from benzene solutions containing an antioxidant, butylhydroxytoluene (~0.1 wt % to the samples), and stored in a deep freezer until use.

The viscoelastic and rheodielectric tests were conducted for the I-1190 and 6(I-179) samples uniformly dissolved in a moderately good solvent, a vinyl-rich oligomeric butadiene B2 (Nisseki PB2000 obtained from Nisseki Co; 1,2-vinyl:1,4-cis/trans = 83:17, $M_w \cong 2\times 10^3$, $M_w/M_n \cong 2$).[26] These PI/B2 systems were prepared by dissolving the prescribed masses of the PI sample and B2 in excess benzene to make ≅5 wt % solutions of PI plus B2 and then allowing benzene to thoroughly evaporate. The PI concentrations were $c_{PI} = 10$ and 15 wt % in the I-1190/B2 systems and $c_{PI} = 20$ and 25 wt % in the 6(I-179)/B2 systems. The number of entanglement segments was $N = M/M_e = 23.8$ and 35.7 for the linear I-1190 chain at $c_{PI} = 10$ and 15 wt % and $N_a = M_a/M_e = 7.2$ and 9.0 for each arm of the star 6(I-179) chain at $c_{PI} = 20$ and 25 wt %. (The entanglement spacing M_e was evaluated as ${M_e}^\circ/\phi_{PI}$, where ${M_e}^\circ$ (= 5×10^3)[1,2] is the M_e in bulk PI and ϕ_{PI} is the PI volume fraction in the PI/B2 systems.)

3.2. Viscoelastic Measurements. For the I-1190/B2 and 6(I-179)/B2 systems, the linear viscoelastic storage and loss moduli G' and G'' were measured at various angular frequencies ω with a laboratory rheometer (ARES, Rheometrics) in a parallel-plate geometry of the plate diameter = 2.5 cm as well as in a cone−plate geometry (rheodielectric cell explained later) of the plate diameter = 5.0 cm and gap angle = 2.0°. The time−temperature superposition worked well at temperatures T between 10 and 90 °C, and the G' and G'' data were reduced at reference temperatures T_r of respective systems (=25 or 30 °C) where the rheodielectric tests were made.

When we examine the nonlinear viscoelastic as well as rheodielectric behavior under steady shear, we need to specify whether the chains (more precisely, the primitive chains) are stretched or not. For this purpose, we conducted the linear viscoelastic measurements for a low-M linear PI sample (I-

Table 2. Linear Viscoelastic Properties of PI/B2 Systems

c_{PI}, wt %	T_r, °C	log τ_{Rouse}, s[a]	log η_0, Pa s	log J_e^0, Pa^{-1}	log $\langle\tau_G\rangle_w$, s
		I-1190/B2 Systems			
10	30	−0.09	4.35	−2.93	1.42
15	30	0.08	5.10	−3.25	1.85
		6(I-179)/B2 Systems			
20	25	−0.65	4.53	−3.41	1.12
25	30	−0.69	4.75	−3.54	1.24

[a] Rouse equilibration time for the primitive chain length of I-1190 and/or 6(I-179) samples. These τ_{Rouse} values were evaluated from the terminal viscoelastic relaxation time of nonentangled low-M linear PI ($M_w = 48.8 \times 10^3$; $M_w/M_n = 1.05$) at respective c_{PI} and T_r (cf. eq 17).

49; $M_w = 48.8 \times 10^3$, $M_w/M_n = 1.05$)[25] dissolved in B2 at c_{PI} = 10, 15, 20, and 25 wt %. This low-M PI was hardly entangled at these c_{PI} values, and its G' and G'' data exhibited Rouse-like ω dependencies. From the terminal viscoelastic relaxation time $\langle\tau_{G,I-49}\rangle_w$ of the I-49 chain evaluated as the product of J_e^0 and η_0, the longest Rouse relaxation time for the length equilibration of the I-1190 and 6(I-179) chains in B2 was estimated as

$$\tau_{Rouse} = 2\left(\frac{M^*}{48.8 \times 10^3}\right)^2 \langle\tau_{G,I-49}\rangle_w \qquad (17)$$

where M^* represents the total molecular weight for the linear I-1190 chain and the span molecular weight $2M_a$ for the star 6(I-179) chain. The prefactor of 2 included in eq 17 accounts for a fact that the length equilibration time is twice of the viscoelastic Rouse relaxation time.

For the I-1190 and/or 6(I-179) chains at respective T_r and c_{PI}, the τ_{Rouse} values obtained from the $\langle\tau_{G,I-49}\rangle_w$ data at the same T_r and c_{PI} are summarized in Table 2. The shear rates examined in this study were smaller than $1/\tau_{Rouse}$, ensuring that the chains were not stretched.

3.3. Dielectric Measurements. The I-1190/B2 and 6(I-179)/B2 systems were charged in a guarded parallel-plate cell with a vacant capacity of C_0 = 120 pF and subjected to the dielectric measurements in the quiescent equilibrium state at various T (= 25−90 °C). In the measurements, we utilized a transformer bridge (1620A, QuadTech) and a homemade circuit,[17] the latter being comprising of a function generator (WF1944, NF Corp.), an electrometer (TR8411, Advantest), and a digital recorder (DL708G, Yokogawa). The bridge was used for high-ω measurements with the current compensation method[22] under a sinusoidally oscillating electric field, and the circuit was utilized for long-time measurements with the adsorption current (AdC) method[17,27,28] under a rectangularly oscillating field.

The time−temperature superposition was valid for the dielectric data obtained at equilibrium, and the shift factor a_T was identical to that for the viscoelastic G' and G'' data. These dielectric data were reduced at T_r of the rheodielectric measurements.

For the I-1190/B2 and 6(I-179)/B2 systems, the rheodielectric measurements under steady shear were made with the AdC method at respective T_r (=25 and/or 30 °C). Measurements at different T values were not attempted for the reason explained later. A narrow-gap, cone−plate type guarded dielectric cell (plate diameter = 5.0 cm, gap angle = 2°, C_0 = 32 pF) was newly designed in this study and utilized in the measurements. Figure 2 schematically shows the cell mounted on the laboratory rheometer (ARES, Rheometrics). The contact ring attached to the cone (moving electrode) was immersed in a mercury reservoir. This reservoir was proved to be very useful for minimizing an electrical noise due to the electrode rotation.[29,30]

The adsorption current $I(t)$ under the steady shear was measured in the shear gradient direction with the rheodielectric cell and the circuit explained above. With the same setup,

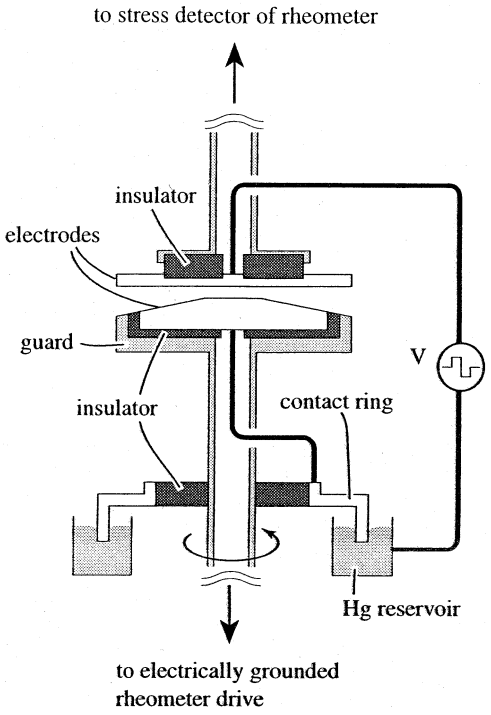

Figure 2. Schematic illustration of a cone−plate type rheodielectric cell mounted on a laboratory rheometer. The plate diameter is 5.0 cm, and the gap angle is 2.0°. The cone and plate electrodes are made of stainless steel, and the cone-head is flattened to ensure no direct contact between the cone and plate. These electrodes are supported by the insulator blocks made of a machinable ceramic. The electrical contact to the moving electrode (cone) is achieved with a stainless steel contact ring immersed in the mercury reservoir. (This ring is supported by a Teflon insulator ring attached to the guard electrode.)

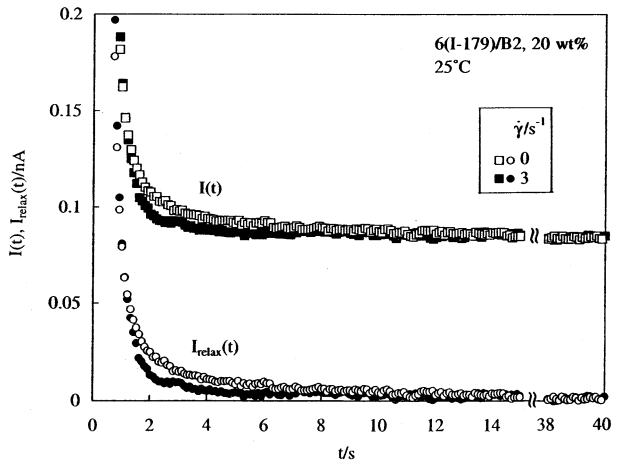

Figure 3. Adsorption current $I(t)$ data obtained for the 6(I-179)/B2 system under the shear at $\dot\gamma = 3\ s^{-1}$ (filled squares) and at equilibrium (unfilled squares). At long t, the current resulting from the chain motion fully relaxed and the $I(t)$ data coincided with the t-independent dc current I_{dc} due to ionic impurities. The relaxational current $I_{relax}(t)$ under the shear and at equilibrium, shown with the filled and unfilled circles, respectively, was obtained by subtracting this I_{dc} from the $I(t)$ data.

$I(t)$ was measured also in a quiescent equilibrium state before and after the shear. Figure 3 shows an example of the $I(t)$ data obtained for the 6(I-179)/B2 system under the shear at $\dot\gamma = 3$ s^{-1} (filled squares) and at equilibrium (unfilled squares; the data before and after the shear were indistinguishable). The half period of the rectangularly oscillating electric field was

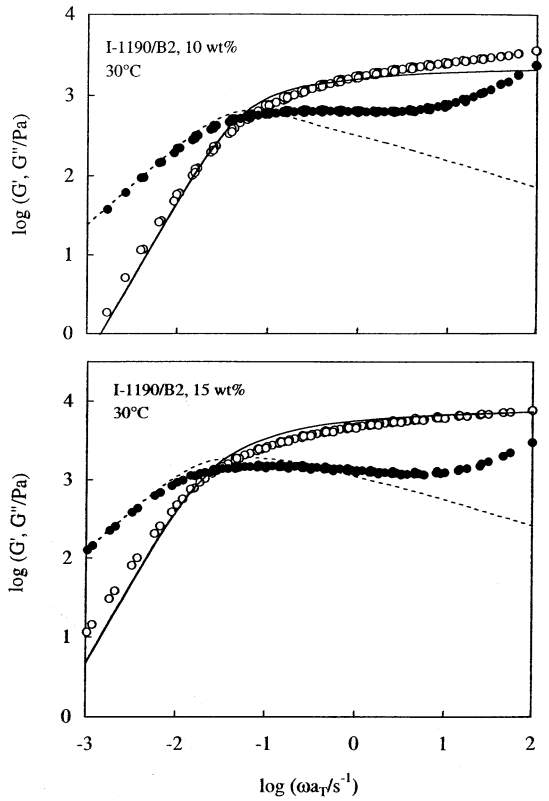

Figure 4. Linear viscoelastic moduli, G' and G'' (unfilled and filled circles), of the I-1190/B2 systems having $c_{PI} = 10$ wt % (top panel) and 15 wt % (bottom panel). The solid and dotted curves indicate the moduli G'_{DTD} and G''_{DTD} calculated from the equilibrium dielectric data (shown in Figures 8 and 9) through the DTD relationship between the viscoelastic and dielectric relaxation functions.

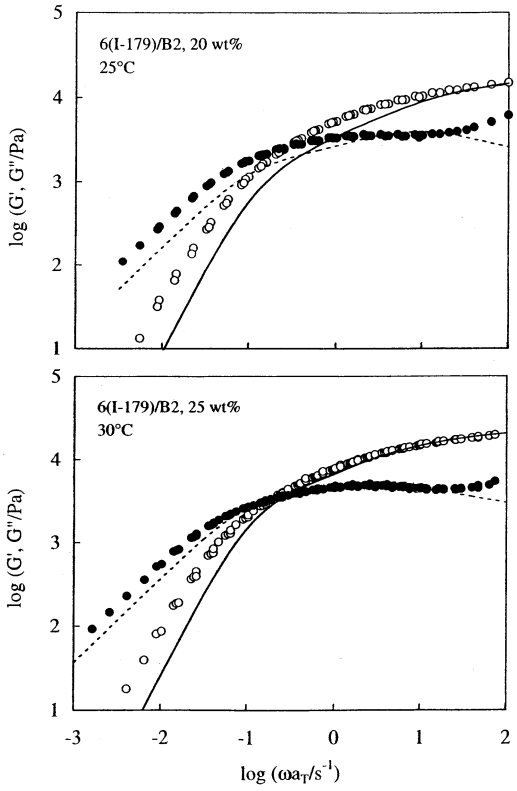

Figure 5. Linear viscoelastic moduli, G' and G'' (unfilled and filled circles), of the 6(I-179)/B2 systems having $c_{PI} = 20$ wt % (top panel) and 25 wt % (bottom panel). The solid and dotted curves indicate the moduli G'_{DTD} and G''_{DTD} calculated from the equilibrium dielectric data (shown in Figures 10 and 11) through the DTD relationship between the viscoelastic and dielectric relaxation functions.

40 s. At sufficiently long t ($\geq 4\langle\tau_G\rangle_w$), the current resulting from the chain motion fully relaxed and the $I(t)$ data coincided with the t-independent dc current I_{dc} due to ionic impurities. Thus, we evaluated the relaxational current $I_{relax}(t) = I(t) - I_{dc}$ (shown with the circles). This $I_{relax}(t)$ was Fourier transformed to obtain the dielectric loss ϵ'' and the relaxational part of the dynamic dielectric constant $\epsilon' - \epsilon_\infty$ (ϵ_∞ = high-frequency dielectric constant). Further details of the measurements with the AdC method were described in our previous paper.[17]

Here, we need to make a comment about the time−temperature superposition. In the quiescent equilibrium state, the superposition is generally valid for the dielectric data reflecting the global motion of PI chains.[15,28] This was the case also for the PI/B2 systems examined in this study.

However, under fast shear, it is rather difficult to make the superposition even for the easiest case of thermorheologically simple materials: If we attempt to make this superposition for the rheodielectric data at various T values, we need to accurately tune the shear rate according to T so as to keep a normalized rate ($\dot{\gamma}a_T$) to be constant. Furthermore, when the dielectric mode distribution changes with the shear rate, i.e., if the shear effect is not the same for fast and slow dielectric modes (which was the case for the star PI chain), the time−temperature superposition itself introduces a conceptual complexity.

Thus, in this study, we measured the rheodielectric signal with the AdC method only at a given T_r (30 or 25 °C) to avoid those difficulty/complexity. Consequently, the rheodielectric data were obtained only at low ω (dominant part of the terminal relaxation), as seen later in Figures 8−11. However, the shear effect was very small for fast dielectric modes, as explained later in more detail. Thus, the rheodielectric data available in the terminal regime were sufficient for our discussion of the shear effect on the chain conformation/dynamics.

4. Results

4.1. Linear Viscoelastic Behavior. In Figures 4 and 5, respectively, the linear viscoelastic moduli G' and G'' (unfilled and filled circles) of the I-1910/B2 and 6(I-179)/B2 systems are plotted against the angular frequency ω. The moduli data are reduced at the reference temperatures T_r of respective systems (where the rheodielectric tests were made). The solid and dotted curves represent the moduli calculated for the dynamic tube dilation process discussed later.

The solvent, B2, had a small viscosity (=13 and 8.7 Pa s at 25 and 30 °C) and exhibited negligibly small elasticity. Thus, the moduli data shown in Figures 4 and 5 are exclusively attributed to the relaxation of the I-1910 and/or 6(I-179) chains. The zero-shear viscosity η_0 ($=[G''/\omega]_{\omega\to 0}$), steady-state compliance J_e^0 ($=[G'/(G'')^2]_{\omega\to 0}$), and the viscoelastic terminal relaxation time $\langle\tau_G\rangle_w$ ($=J_e^0\eta_0$), evaluated from the moduli data, are summarized in Table 2.

The viscoelastic mode distribution is much broader for the star 6(I-179) chain than for the linear I-1190 chain (cf. Figures 4 and 5), reflecting a difference in their equilibrium relaxation mechanisms: The tube models consider that the slow relaxation of the linear chain occurs through reptation in a dynamically dilated tube[18,31] while the star arm relaxes via its retraction along the dilated tube.[19,20] This difference can naturally lead to the observed difference in the mode distribution. The dynamic tube dilation (DTD) mechanism incorporated in these models is discussed later in relation to the rheodielectric behavior of the linear/star PI chains.

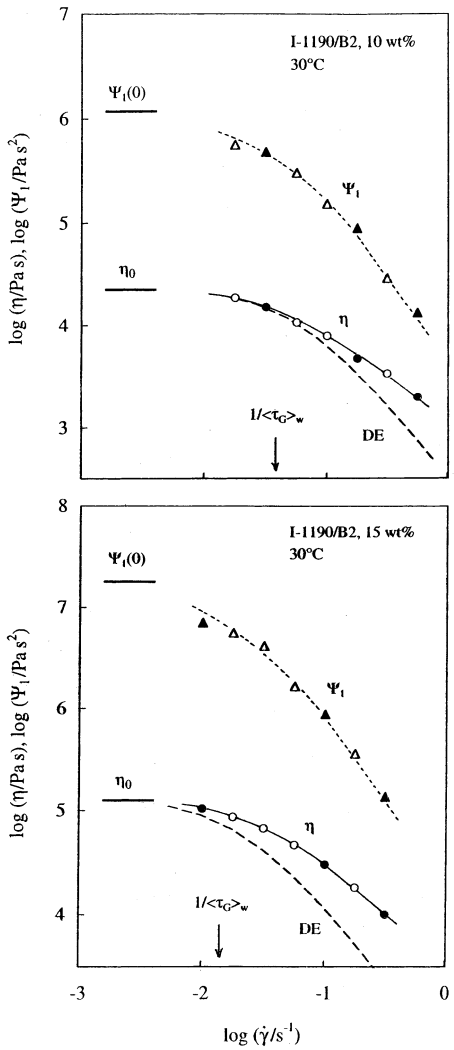

Figure 6. Steady-state viscosity η and first normal stress coefficient Ψ_1 of the I-1190/B2 systems having c_{PI} = 10 wt % (top panel) and 15 wt % (bottom panel). The horizontal thick solid lines indicate the zero-shear values η_0 and $\Psi_1(0)$. The dashed curves indicate the η_{DE} calculated from the Doi−Edwards constitutive equation. For further details, see the text.

4.2. Nonlinear Flow Behavior. Figures 6 and 7 show the viscosity η and the first normal stress coefficient Ψ_1 of the I-1190/B2 and 6(I-179)/B2 systems at T_r as indicated. The solvent B2 (having $\eta_0 \leq 13$ Pa s at these T_r) negligibly contributes to the η and Ψ_1 data, and these data are exclusively attributed to the viscous dissipation and elastic energy storage of the I-1190 and 6(I-179) chains under the shear. These data were obtained with the cone−plate type rheodielectric cell (cf. Figure 2), and the rheodielectric measurements were made at representative shear rates. The η and Ψ_1 data obtained at these rates are shown in Figures 6 and 7 with the filled symbols.

In Figures 6 and 7, the horizontal lines indicate the zero-shear viscosity η_0 and zero-shear coefficient $\Psi_1(0)$ ($=2\eta_0^2 J_e^0$); cf. Table 2. The η and Ψ_1 data significantly decrease from respective zero-shear values as the shear rate $\dot{\gamma}$ is increased above the equilibrium viscoelastic relaxation frequency $1/\langle\tau_G\rangle_w$ (arrows). The $\dot{\gamma}$ dependencies of these nonlinear η and Ψ_1 data are very similar to those reported for various entangled systems.[1,2,32−35]

It should be emphasized that the shear rates examined in Figures 6 and 7 are smaller than the Rouse

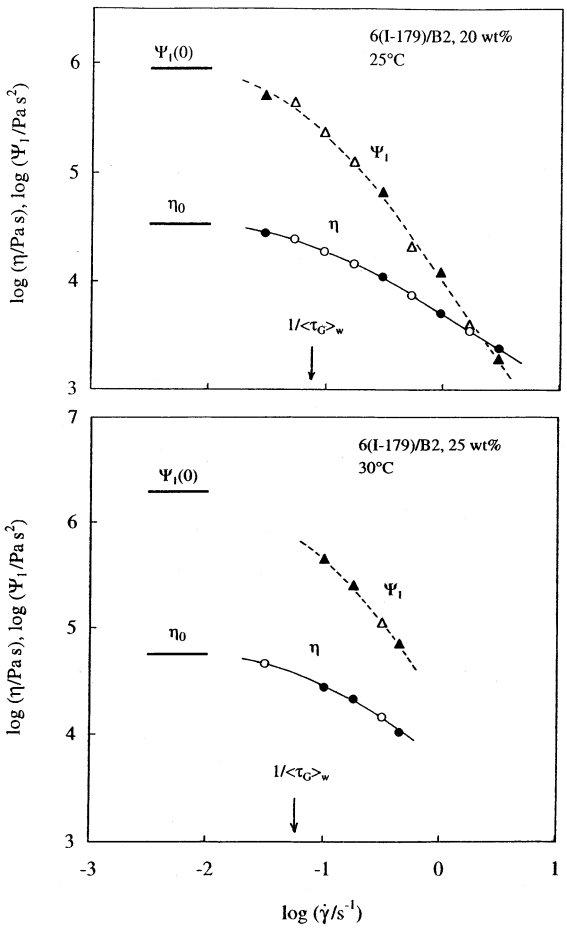

Figure 7. Steady-state viscosity η and first normal stress coefficient Ψ_1 of the 6(I-179)/B2 systems having c_{PI} = 20 wt % (top panel) and 25 wt % (bottom panel). The horizontal thick solid lines indicate the zero-shear values η_0 and $\Psi_1(0)$.

frequency $1/\tau_{Rouse}$ (cf. Table 2) for the equilibration of the primitive chain length. Thus, the chain is not stretched but orientated to exhibit the significant nonlinearities of η and Ψ_1.

For such nonstretched linear chains, Doi and Edwards (DE) formulated a reptation-based constitutive equation under the independent alignment approximation (IAA):[4]

$$\boldsymbol{\sigma}(t) = G_N \int_{-\infty}^{t} \frac{\partial \mu(t-t')}{\partial t'} \mathbf{Q}^{IAA}(\boldsymbol{E}_{t,t'})\, dt' \qquad (18)$$

Here, $\mu(t)$ ($=G(t)/G_N$) is the normalized linear viscoelastic relaxation function, $\boldsymbol{E}_{t,t'}$ is the displacement tensor between the two times t' and t, and $\mathbf{Q}^{IAA}$ is the IAA-type DE tensor.[4] Utilizing an approximate single-mode relaxation function $\mu(t) = \exp(-t/\langle\tau_G\rangle_w)$ in eq 18, we calculated the DE viscosity η_{DE} for the linear I-1190 chain; see the dashed curves in Figure 6. The decrease of η_{DE} with $\dot{\gamma}$ is much stronger than that of the η data. This problem cannot be removed even if the empirical $\mu(t)$ having the mode distribution is utilized in eq 18. The same problem emerges also for the star chain, if we assume the unleakable/undilated tube for the star arm.

The above problem results from the very strong shear-orientation of the chain deduced from the DE model. The convective constraint release (CCR) mechanism,[8−10] which allows the lateral leakage from the tube under shear thereby weakening the shear-orientation, is es-

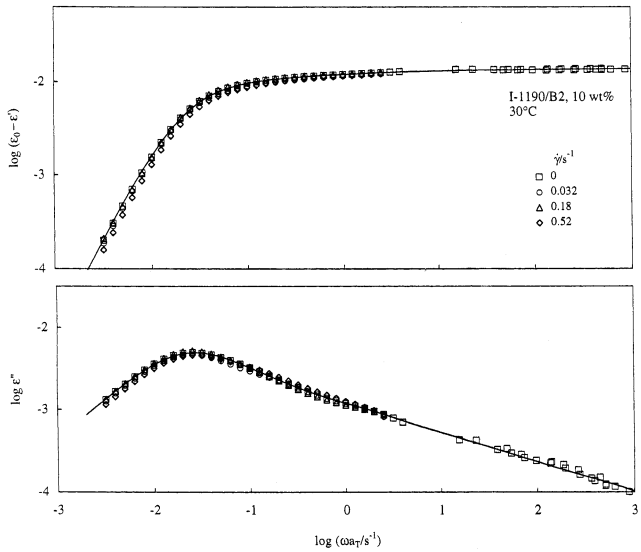

Figure 8. Rheodielectric behavior of the 10 wt % I-1190/B2 system under the steady shear at the rates $\dot{\gamma}$ as indicated. The data for $\dot{\gamma} = 0$ were obtained in the quiescent equilibrium state.

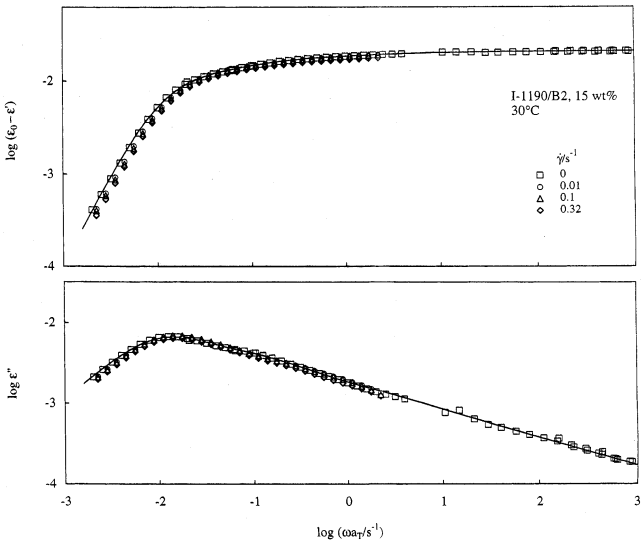

Figure 9. Rheodielectric behavior of the 15 wt % I-1190/B2 system under the steady shear at the rates $\dot{\gamma}$ as indicated. The data for $\dot{\gamma} = 0$ were obtained in the quiescent equilibrium state.

sential for the refinement of the model. This mechanism is discussed later in relation to the rheodielectric data.

4.3. Rheodielectric Behavior. 4.3.1. Overview. Figures 8−11 show the dielectric behavior of the I-1190/B2 and 6(I-179)/B2 systems in the quiescent equilibrium state ($\dot{\gamma} = 0$) and under steady shear at the rates as indicated. The $\epsilon_0 - \epsilon'$ and ϵ'' data are double-logarithmically plotted against the angular frequency ω. From these data, we evaluated the dielectric intensity $\Delta\epsilon$ (eq 14), the terminal dielectric relaxation time $\langle\tau_\epsilon\rangle_w$ (eq 15), and the dielectric compliance ϑ_ϵ (eq 16).

Since the solvent B2 has no type-A dipoles, the dielectric relaxation seen in Figures 8−11 is exclusively attributed to the global motion of the I-1190 and/or 6(I-179)/B2 chains.[36] Under the shear, the chains are oriented on average but their end-to-end vectors **R** are fluctuating with time. This fluctuation, resulting in a decay of the memory of the chain conformation at a past time during the steady shear, is detected as the dielectric relaxation.

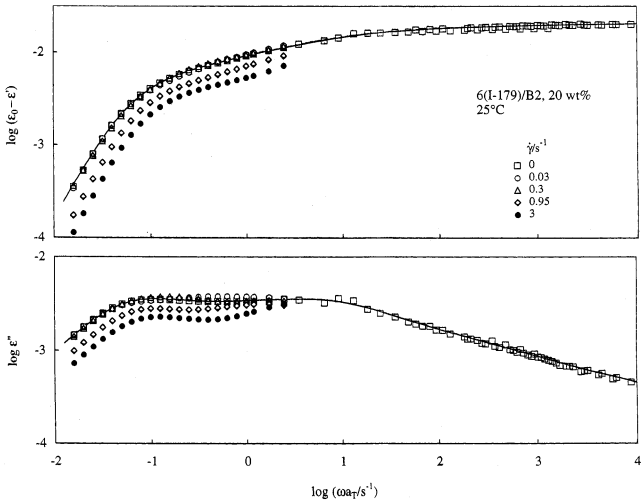

Figure 10. Rheodielectric behavior of the 20 wt % 6(I-179)/B2 system under the steady shear at the rates $\dot{\gamma}$ as indicated. The data for $\dot{\gamma} = 0$ were obtained in the quiescent equilibrium state.

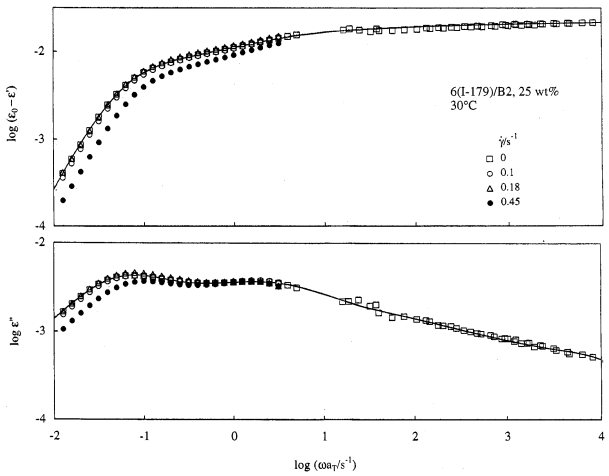

Figure 11. Rheodielectric behavior of the 25 wt % 6(I-179)/B2 system under the steady shear at the rates $\dot{\gamma}$ as indicated. The data for $\dot{\gamma} = 0$ were obtained in the quiescent equilibrium state.

The ω dependence of the $\epsilon_0 - \epsilon'$ and ϵ'' data reflect the dielectric mode distribution. Comparing the data for the linear I-1190 and star 6(I-179) chains at equilibrium (unfilled squares in Figures 8−11), we note that the mode distribution is much broader for the latter. In fact, this difference was quantitatively confirmed for the product $\vartheta_\epsilon\Delta\epsilon$ (the measure of the mode distribution); $\vartheta_\epsilon\Delta\epsilon \cong 1.8$ for the I-1190 chain, and $\vartheta_\epsilon\Delta\epsilon \cong 3$ for the 6(I-179) chain.

The equilibrium mode distribution of the star 6(I-179) chain is characterized with two broad peaks of ϵ''; see Figures 10 and 11. The high-ω peak is observed at $\omega \cong 1/\tau_{\text{Rouse}}$ (cf. Table 2) and attributed to the Rouse-like equilibration of the arm length.[17] On the other hand, the ϵ'' peak at low ω is attributable to the thermal constraint release (TCR) motion and not to the full retraction of the arm along the dilated tube, as discussed in our previous paper.[17]

Now, we turn our attention to the rheodielectric feature under the steady shear. We first note that the $\epsilon_0 - \epsilon'$ and ϵ'' data of the linear I-1190 chain are hardly affected by the shear; see Figures 8 and 9. This result is surprising in some sense, because significant thinning

is observed for the viscoelastic η and Ψ_1 data in the same range of $\dot{\gamma}$; see Figure 6.

In contrast, the star 6(I-179) chain exhibits detectable rheodielectric changes; see Figures 10 and 11. The height of the low-ω ϵ'' peak is decreased with increasing $\dot{\gamma}$ and $\Delta\epsilon$ decreases accordingly, while the terminal dielectric relaxation is accelerated. These rheodielectric changes are noted also from the raw adsorption current data; see Figure 3.

It should be emphasized that these shear-induced changes are observed only at low ω. With increasing ω toward the Rouse frequency $1/\tau_{\text{Rouse}}$ where the high-ω ϵ'' peak is observed, the ϵ'' data for $\dot{\gamma} > 0$ approach the equilibrium data and the shear effect vanishes; see Figures 10 and 11. This fact suggests that the fast dielectric modes having the relaxation times $\tau_p < \tau_{\text{Rouse}}$ are not affected by the shear at $\dot{\gamma} < 1/\tau_{\text{Rouse}}$.

As seen in the top panels of Figures 10 and 11, the $\epsilon_0 - \epsilon'$ data of the star chain under the fast shear do not approach the equilibrium data even when ω is increased to $1/\tau_{\text{Rouse}}$. One might attribute this result to the shear effect on the fast dielectric modes. However, this is not the case: The $\epsilon_0 - \epsilon'$ approaches $\Delta\epsilon$ with increasing ω (cf. eq 13), and the deviation of the $\epsilon_0 - \epsilon'$ data for large and small $\dot{\gamma}$ seen at $\omega \cong 1/\tau_{\text{Rouse}}$ is attributed to the shear-induced decrease of $\Delta\epsilon$. This decrease of $\Delta\epsilon$ results from the decreases of the intensities of the slow dielectric modes having $\tau_p > \tau_{\text{Rouse}}$. Namely, the above deviation of the $\epsilon_0 - \epsilon'$ data reflects the shear effects on the slow modes.

4.3.2. Rheodielectric Changes. The $\langle\tau_\epsilon\rangle_w$ and ϑ_ϵ are determined only from the dielectric data at low ω where the terminal tails ($\epsilon_0 - \epsilon' \propto \omega^2$ and $\epsilon'' \propto \omega$) are observed; see eqs 15 and 16. These tails are seen for the $\epsilon_0 - \epsilon'$ and ϵ'' data of all PI/B2 systems at all $\dot{\gamma}$ values; cf. Figures 8-11. Thus, we utilized these data to evaluate $\langle\tau_\epsilon\rangle_w$ and ϑ_ϵ^{-1} (terminal dielectric intensity).

In contrast, the evaluation of the total dielectric intensity $\Delta\epsilon$ requires us to have the ϵ'' data in the entire range of ω between 0 and ∞ (cf. eq 14). Obviously, the ϵ'' data were obtained in a finite range of ω. Thus, we introduced extrapolating functions to evaluate $\Delta\epsilon$ in the following way.

For the $\Delta\epsilon(0)$ at equilibrium ($\dot{\gamma} = 0$), these functions can be easily chosen. The dielectric relaxation was completed already in the low-ω side of our experimental window, as noted from the observed terminal tail ($\epsilon'' \propto \omega$). Thus, at lower ω out of our window, ϵ'' should be described by

$$\epsilon'' = K_{\text{low}}\omega \quad \text{at low } \omega \tag{19}$$

We utilized eq 19 as the low-ω extrapolating function, with the prefactor K_{low} being determined from the ϵ'' data in the low-ω side of our window.

In the high-ω side of our window, the ϵ'' data at equilibrium are well described by a power-law function (cf. Figures 8−11)

$$\epsilon'' = K_{\text{high}}\omega^{-m} \quad \text{at high } \omega \tag{20}$$

This function was utilized as the high-ω extrapolating function, with the prefactor K_{high} and exponent m being evaluated from those data for respective systems.

The intensity $\Delta\epsilon(0)$ was evaluated as a sum of the numerical integral of the ϵ'' data and analytical integrals of eqs 19 and 20, with the latter two integrals being calculated in the low and high ω ranges not covered in our experiments. It turned out that the contribution of these analytical integrals to $\Delta\epsilon$ was minor because the ϵ'' data were measured in a considerably wide range of ω.

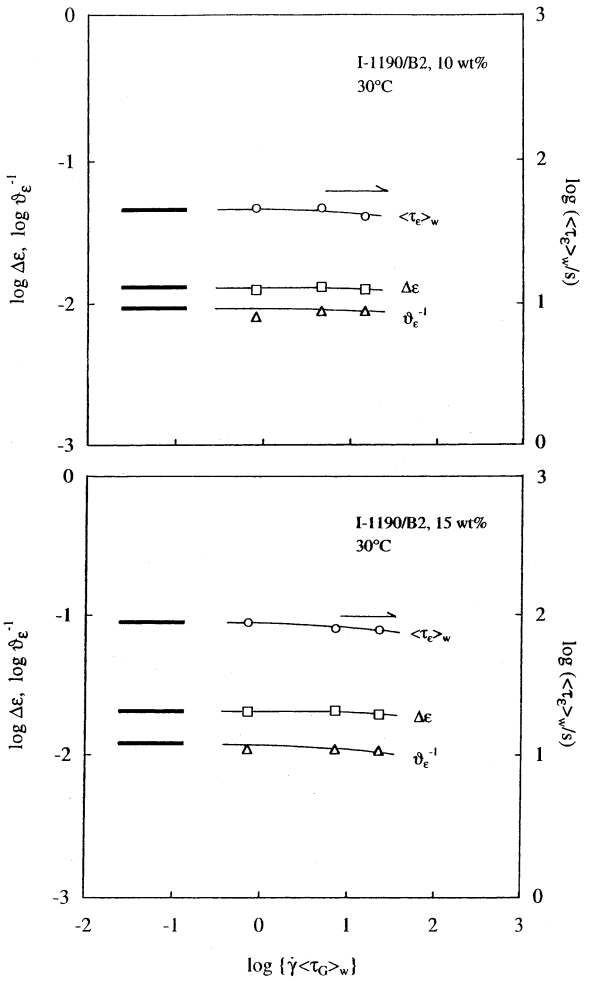

Figure 12. Dependence of the total and terminal dielectric intensities, $\Delta\epsilon$ and ϑ_ϵ^{-1}, and terminal dielectric relaxation time, $\langle\tau_\epsilon\rangle_w$, of the I-1190/B2 systems (c_{PI} = 10 and 15 wt %) on the normalized shear rate $\dot{\gamma}\langle\tau_G\rangle_w$. The horizontal thick lines indicate the equilibrium values of respective quantities.

Under the shear, the ϵ'' data are available only in the terminal regime and the high-ω extrapolating function cannot be determined from these data. However, with increasing ω up to the highest frequency ω_h examined under the shear, the ϵ'' data for $\dot{\gamma} > 0$ become very close to those at equilibrium; see Figures 8−11. Considering this fact, we evaluated the intensity under the shear as $\Delta\epsilon(\dot{\gamma}) = \Delta\epsilon_1 + \Delta\epsilon_m + \Delta\epsilon_h$, where $\Delta\epsilon_1$ is an analytical integral of the low-ω extrapolating function (eq 19 with K_{low} being evaluated from the low-ω data under the shear), $\Delta\epsilon_m$ is a numerical integral of the ϵ'' data under the shear, and $\Delta\epsilon_h$ is an integral of the *equilibrium* ϵ'' data at $\omega > \omega_h$. This $\Delta\epsilon_h$ was obtained as a sum of the numerical integral of these equilibrium data and the analytical integral of the high-ω extrapolating function (eq 20).

In Figures 12 and 13, the $\langle\tau_\epsilon\rangle_w$, ϑ_ϵ^{-1}, and $\Delta\epsilon$ data thus obtained for the I-1190 and 6(I-179) chains are double-logarithmically plotted against a normalized shear rate $\dot{\gamma}\langle\tau_G\rangle_w$. The horizontal thick lines indicate the equilibrium values of these quantities. (The dielectric $\langle\tau_\epsilon\rangle_w$ at equilibrium was close to the viscoelastic $\langle\tau_G\rangle_w$, as noted also for bulk PI systems.[12,15,17])

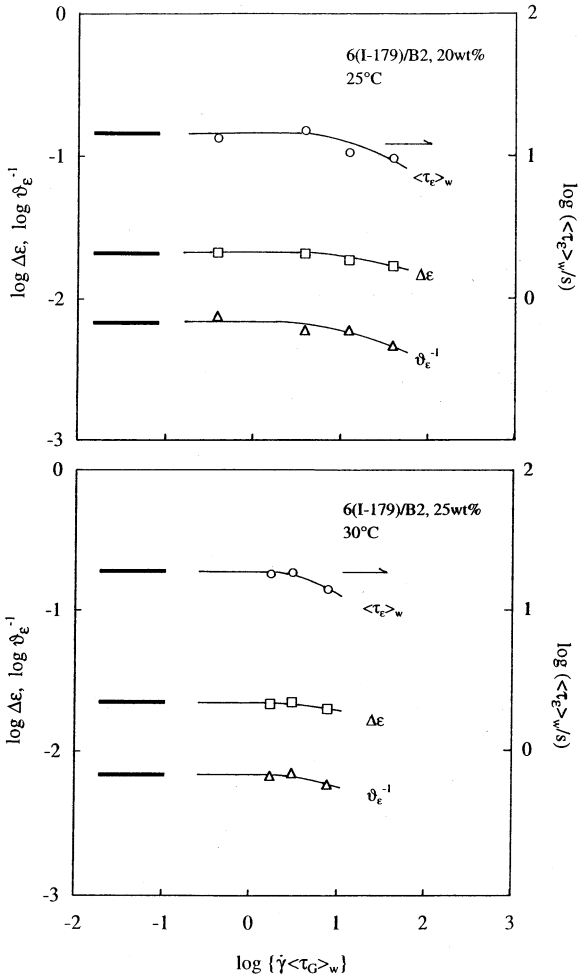

Figure 13. Dependence of the total and terminal dielectric intensities, $\Delta\epsilon$ and ϑ_ϵ^{-1}, and terminal dielectric relaxation time, $\langle\tau_\epsilon\rangle_w$, of the 6(I-179)/B2 systems (c_{PI} = 20 and 25 wt %) on the normalized shear rate $\dot{\gamma}\langle\tau_G\rangle_w$. The horizontal thick lines indicate the equilibrium values of respective quantities.

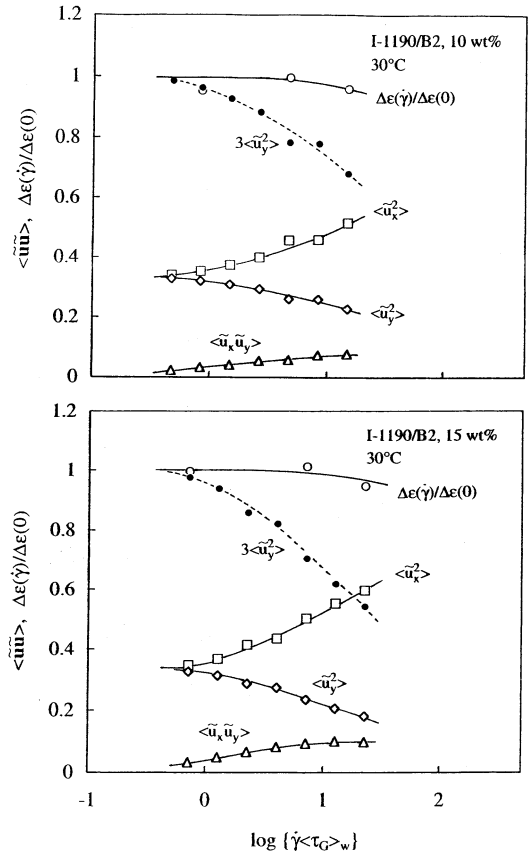

Figure 14. Dependence of the components of the dyadic $\langle\tilde{\mathbf{u}}\tilde{\mathbf{u}}\rangle$ and the normalized dielectric intensity $\Delta\epsilon(\dot{\gamma})/\Delta\epsilon(0)$ of the I-1190/B2 systems (c_{PI} = 10 and 15 wt %) on the normalized shear rate $\dot{\gamma}\langle\tau_G\rangle_w$.

As seen in Figure 13, the $\langle\tau_\epsilon\rangle_w$, ϑ_ϵ^{-1}, and $\Delta\epsilon$ data of the star 6(I-179) chain exhibit moderate decreases (by factors of ≅40%, 30%, and 20%, respectively) with increasing $\dot{\gamma}$ up to $40/\langle\tau_G\rangle_w$. These decreases can be noted also from the raw adsorption current data; see Figure 3. However, it should be emphasized that the viscoelastic η and Ψ_1 exhibit order-of-magnitude decreases; see Figure 7. Thus, the dielectric response (in the shear gradient direction) is much less sensitive to the shear than the viscoelastic response.

For the linear I-1190 chain, the $\langle\tau_\epsilon\rangle_w$, ϑ_ϵ^{-1}, and $\Delta\epsilon$ data decrease by a factor of ≅10% with increasing $\dot{\gamma}$ up to $30/\langle\tau_G\rangle_w$; see Figure 12. These decreases are weaker than those seen for the star chain. Thus, the shear effect is considerably different for the star and linear chains, as already noted from the comparison of Figures 8−11. This difference is later discussed in relation to a difference in the equilibrium DTD processes for the linear and star chains.

4.3. Chain Conformation under Steady Shear. Applying eqs 3 and 4 to the η and Ψ_1 data of the I-1190 and 6(I-179) chains of various c_{PI} (Figures 6 and 7), we evaluated the averages of the bond vector components of the entanglement segments, $\langle\tilde{u}_x\tilde{u}_y\rangle$ and $\langle\tilde{u}_x^2\rangle - \langle\tilde{u}_y^2\rangle$. The G_N data (in Pa) utilized in this evaluation were 0.48×10^4, 1.1×10^4, 1.9×10^4, and 3.0×10^4 for c_{PI} = 10, 15, 20, and 25 wt %, respectively.

The second normal stress coefficient Ψ_2 was not measured in our experiments. However, literature data for entangled solutions of linear chains[33−35] allowed us to estimate Ψ_2 of the I-1190 linear chain: At the high shear rates where the rheodielectric data were measured for this chain, the first normal stress difference N_1 ($=\Psi_1\dot{\gamma}^2$) was close to twice of the shear stress $2\sigma_s$ ($=2\eta\dot{\gamma}$). Under such conditions, Ψ_2 of entangled linear chains of various entanglement densities is close to $-0.1\Psi_1$.[33−35] Thus, we estimated Ψ_2 of our I-1190 chain to be $-0.1\Psi_1$ (with the Ψ_1 data shown in Figure 6) and utilized this Ψ_2 in eq 5 to estimate the value of $\langle\tilde{u}_x^2\rangle + 2\langle\tilde{u}_y^2\rangle - 1$. Combining this value with the $\langle\tilde{u}_x^2\rangle - \langle\tilde{u}_y^2\rangle$ value determined above, we obtained the values of $\langle\tilde{u}_x^2\rangle$ and $\langle\tilde{u}_y^2\rangle$.

No literature data were found for Ψ_2 of entangled star chains sheared under the conditions similar to those for our 6(I-179) chain. However, the $\dot{\gamma}$ dependencies of the η and Ψ_1 data are similar for the star 6(I-179) and linear I-1190 chains (cf. Figures 6 and 7), and N_1 was close to $2\sigma_s$ also for the star chain. Under the lack of the information about Ψ_2 of the star 6(I-179) chain, we assumed the relationship $\Psi_2 \cong -0.1\Psi_1$ to estimate $\langle\tilde{u}_x^2\rangle$ and $\langle\tilde{u}_y^2\rangle$ of this chain.

In Figures 14 and 15, the $\langle\tilde{u}_x\tilde{u}_y\rangle$, $\langle\tilde{u}_x^2\rangle$, and $\langle\tilde{u}_y^2\rangle$ thus evaluated are semilogarithmically plotted against the normalized shear rate $\dot{\gamma}\langle\tau_G\rangle_w$; see unfilled triangles, squares, and diamonds. To examine the accuracy of these $\langle\tilde{u}_x^2\rangle$ and $\langle\tilde{u}_y^2\rangle$ values (obtained from $\Psi_2 \cong -0.1\Psi_1$), we estimated $\langle\tilde{u}_x^2\rangle$ and $\langle\tilde{u}_y^2\rangle$ for the two extreme cases of Ψ_2, $\Psi_2 \cong -0.2\Psi_1$ (zero-shear limit) and $\Psi_2 \cong 0$ (high-shear limit). For both cases, the estimated $\langle\tilde{u}_x^2\rangle$ and $\langle\tilde{u}_y^2\rangle$

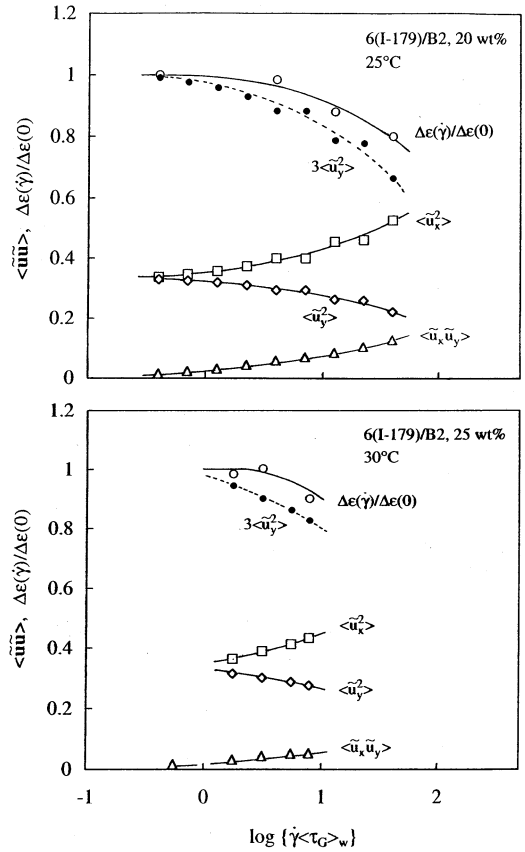

Figure 15. Dependence of the components of the dyadic $\langle \tilde{\mathbf{u}}\tilde{\mathbf{u}} \rangle$ and the normalized dielectric intensity $\Delta\epsilon(\dot{\gamma})/\Delta\epsilon(0)$ of the 6(I-179)/B2 systems (c_{PI} = 20 and 25 wt %) on the normalized shear rate $\dot{\gamma}\langle\tau_G\rangle_w$.

were not significantly different from those for $\Psi_2 \cong -0.1\Psi_1$. Thus, the $\langle \tilde{u}_x^2 \rangle$ and $\langle \tilde{u}_y^2 \rangle$ data shown in Figures 14 and 15 can be safely utilized to discuss the chain conformation under the steady shear.

As seen in Figures 14 and 15, $\langle \tilde{u}_x^2 \rangle$ and $\langle \tilde{u}_y^2 \rangle$ increases and decreases, respectively, from their zero-shear values ($=^1/_3$) as $\dot{\gamma}$ is increased above $1/\langle\tau_G\rangle_w$. Correspondingly, $\langle \tilde{u}_x\tilde{u}_y \rangle$ increases with $\dot{\gamma}$. These results indicate that the I-1190 and 6(I-179) chains are shear-oriented. However, this orientation is not very large; the extinction angle representing an average orientation direction, $\chi = 0.5 \tan^{-1}\{2\langle \tilde{u}_x\tilde{u}_y \rangle/(\langle \tilde{u}_x^2 \rangle - \langle \tilde{u}_y^2 \rangle)\} = 0.5 \tan^{-1}\{2\sigma_s/N_1\}$, remains well above 10° for the linear/star chains even at the largest $\dot{\gamma}$ examined. This rather weak orientation is in harmony with the results of SANS observation of the conformation of sheared polystyrene chains[37] (although the radius of gyration in the shear gradient direction obtained from SANS is not equivalent to the dielectrically measured end-to-end distance $\langle R_y^2 \rangle^{1/2}$.) Concerning this point, we confirmed that the above χ value is larger than that calculated from the DE model.[4]

In Figures 14 and 15, the normalized dielectric intensity $\Delta\epsilon(\dot{\gamma})/\Delta\epsilon(0)$ is shown with the unfilled circles. For the linear I-1190 chain (Figure 14), this $\Delta\epsilon(\dot{\gamma})/\Delta\epsilon(0)$ is significantly larger than $3\langle \tilde{u}_y^2 \rangle$ (filled circles), meaning that some successive entanglement segments have a strong isochronal cross-correlation in their orientation; see the $(\beta - 1)\langle \tilde{u}_y\tilde{u}_y' \rangle$ term in eq 12. For the star 6(I-179) chain (Figure 15), the difference between $\Delta\epsilon(\dot{\gamma})/\Delta\epsilon(0)$ and $3\langle \tilde{u}_y^2 \rangle$ is smaller and the cross-correlation is weaker. However, at the largest $\dot{\gamma}$ examined, this difference is well above the uncertainties in our experiments/analyses and the existence of the isochronal cross-correlation under high shear is concluded also for the star chain.

5. Discussion

The difference between the $\Delta\epsilon(\dot{\gamma})/\Delta\epsilon(0)$ and $3\langle \tilde{u}_y^2 \rangle$ data (Figures 14 and 15) unequivocally indicates that a sequence of entanglement segments exhibits the isochronal orientational cross-correlation under the fast shear. Unfortunately, these data alone do not allow us to separately estimate the segment number β and the magnitude of correlation $\langle \tilde{u}_y\tilde{u}_y' \rangle$ in this sequence, because no general relationship between $\langle \tilde{u}_y^2 \rangle$ and $\langle \tilde{u}_y\tilde{u}_y' \rangle$ is available. However, we may make this separate estimation on the basis of a molecular argument explained below.

The cross-correlation of the *shear-oriented* segments would emerge when they are mutually equilibrated. (In other words, the segments would be orientated in an uncorrelated way if this equilibration does not occur.) The mutual equilibration due to the shear would occur through the dynamic tube dilation (DTD) that is induced by the convective constraint release (CCR). Thus, β and $\langle \tilde{u}_y\tilde{u}_y' \rangle$ may be separately estimated with the aid of a relationship between $\langle \tilde{u}_y^2 \rangle$ and $\langle \tilde{u}_y\tilde{u}_y' \rangle$ derived from the CCR−DTD molecular picture.

This CCR-induced DTD (under the shear) is intimately related to the equilibrium DTD induced by the thermal constraint release (TCR) due to the equilibrium chain motion. A difference is found for the TCR−DTD processes of the linear and star chains at equilibrium,[14,17] and this difference would be responsible for the difference of the shear-induced cross-correlation observed for the linear and star chains (Figures 14 and 15).

In the remaining part of this paper, we first focus on this importance of the TCR−DTD process and summarize the TCR−DTD behavior of the linear and star chains. Then, in relation to this behavior, we discuss the difference in the nonequilibrium CCR−DTD processes of these chains under the shear. Furthermore, we derive a CCR−DTD relationship between $\langle \tilde{u}_y^2 \rangle$ and $\langle \tilde{u}_y\tilde{u}_y' \rangle$ to estimate β and $\langle \tilde{u}_y\tilde{u}_y' \rangle$ separately.

5.1. TCR—DTD at Equilibrium. At equilibrium, DTD is equivalent to the mutual equilibration of successive entanglement segments due to TCR. Thus, the molecular picture of DTD is valid only in time scales longer than the time necessary for the TCR-induced equilibration.

Concerning this point, we recently examined the validity of a DTD relationship between the viscoelastic and dielectric relaxation functions of monodisperse type-A chains,[12,13,17] $G(t)/G_N \cong [\Phi(t)]^2$. This relationship was found to hold in the terminal regime of linear PI chains[13,16,17] but not for star PI chains.[12,14,17] The same result is confirmed for the linear and star PI chains examined in this study: In Figures 4 and 5, the solid and dotted curves indicate G'_{DTD} and G''_{DTD} calculated from the equilibrium dielectric data (Figures 8−11) through the above DTD relationship. In the dominant part of the terminal relaxation, these DTD curves are close to the data for the linear I-1190 chains (Figure 4), but a significant deviation is noted for the star 6(I-179) chain (Figure 5).

The success of the DTD picture for the linear chain at equilibrium is related to its narrowly distributed motional modes that allow $\Phi(t)$ to remain rather large

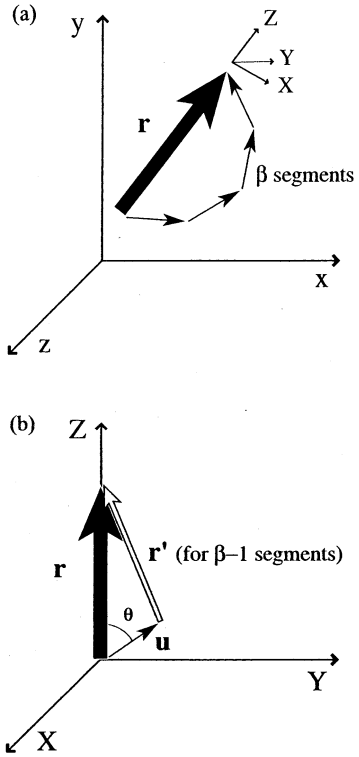

Figure 16. Schematic illustration of a sequence of β entanglement segments (subchain) having a given end-to-end vector **r** (thick arrow). In both parts a and b, thin arrows indicate the bond vectors of these segments. For the given **r**, the average of the squared component of the unit bond vector $\langle \tilde{u}_r^2 \rangle_r$ is calculated from a distribution function $W(\mathbf{r}')$ of an end-to-end vector $\mathbf{r}'$ of a subsequence composed of $\beta - 1$ segments (cf. part b).

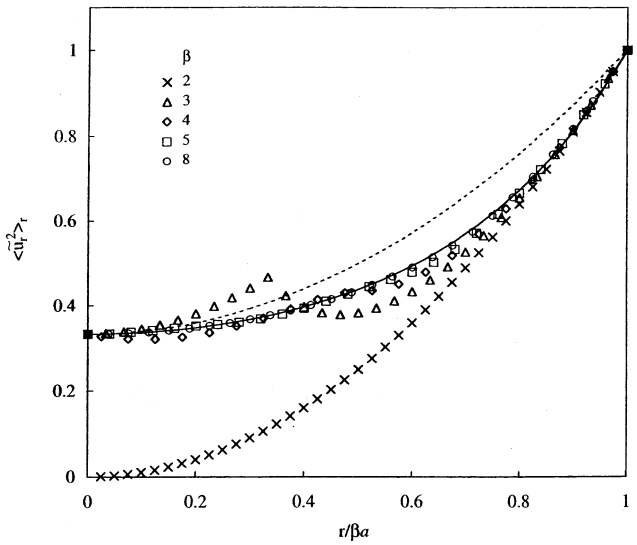

Figure 17. Plots of the average of the squared component of the unit vector of the entanglement segments, $\langle \tilde{u}_r^2 \rangle_r$ evaluated for a given end-to-end distance r, against the reduced distance $r/\beta a$. The plots are shown for several β values ≤ 8. (The plots for $\beta \geq 9$ were collapsed on the solid curve and indistinguishable from the plot for $\beta = 8$). For further details, see the text.

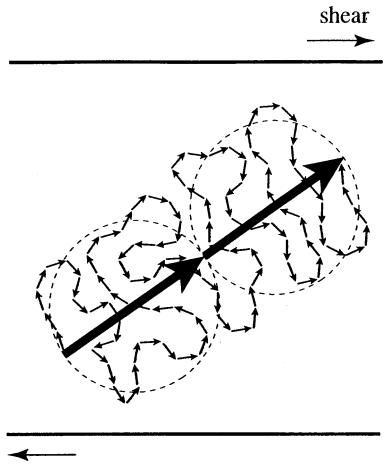

Figure 18. Schematic illustration of two entanglement segments that are not stretched but coherently oriented in the direction of the subchain axis under fast shear. Thick arrows indicate the bond vectors **u** of these segments, and thin arrows indicate monomeric bond vectors. Since each entanglement segment includes many monomeric units, the monomeric bond vectors have a vanishingly small isochronal cross-correlation in their orientation.

even at long $t \cong \langle \tau_\epsilon \rangle_w$ (terminal dielectric relaxation time):[14,17] For this $\Phi(t)$, the dilated tube diameter $a' \cong a[\Phi(t)]^{-1/2}$ is rather small and the required TCR-equilibration time $\tau^{**} \propto [a'/a]^4 \propto [\Phi(t)]^{-2}$ remains rather short even at $t \cong \langle \tau_\epsilon \rangle_w$. Then, the tube actually dilates in time, leading to the success of the DTD picture.

Correspondingly, the failure of the DTD picture for the star chain is related to its broadly distributed motional modes giving a considerably small $\Phi(t)$ value at $t \cong \langle \tau_\epsilon \rangle_w$:[14,17] For this case, τ^{**} becomes longer than t in the terminal regime and the tube cannot dilate in time, resulting in the failure of the DTD picture. Thus, for the star arm at equilibrium, the tube dilates to a certain large diameter a_c' ($> a'$ for the linear chain) with increasing t up to a critical time t_c, and the arm motion at longer t ($> t_c$) is quite possibly dominated by the TCR mechanism.[17]

This terminal TCR process has a large dielectric intensity but an undetectably small viscoelastic intensity, as suggested from our recent analysis.[17] Thus, the viscoelastic relaxation of the star chains is *practically* completed in a range of $t < t_c$ via the arm retraction along the dilated tube, thereby allowing the tube model considering this retraction[20] to describe the viscoelastic data. However, the arm motion itself is not completed through this retraction (as noted from the dielectric data) and the real terminal motion of the arm occurs through the TCR mechanism.[17]

5.2. CCR—DTD under Steady Shear. Under the shear, the CCR mechanism enlarges the dilated tube diameter a' (above the diameter at equilibrium), thereby enhancing the mutual equilibration of the segments and inducing the isochronal cross-correlation. At equilibrium, a' is smaller for the linear chain than for the star chain. Thus, the shear-induced dilation/equilibration would occur more easily to give the stronger cross-correlation for the linear chain. This difference between the linear and star chains is further discussed later in relation to Figure 19.

On the basis of this CCR−DTD molecular picture, we attempted to separately estimate β and $\langle \tilde{u}_y \tilde{u}_y' \rangle$. For this purpose, we analyzed the orientation distribution of the correlated segments to derive a relationship between $\langle \tilde{\mathbf{u}} \tilde{\mathbf{u}} \rangle$ of these segments and the orientational anisotropy of the sequence of the segments as a whole. Then, we utilized this relationship to derive a CCR−DTD relationship between $\langle \tilde{u}_y \tilde{u}_y' \rangle$ and $\langle \tilde{u}_y^2 \rangle$ and separately estimated β and $\langle \tilde{u}_y \tilde{u}_y' \rangle$. Details of these results are described below.

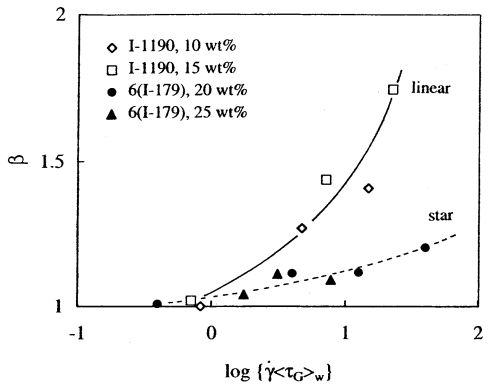

Figure 19. Number β of entanglement segments that are mutually equilibrated through the CCR−DTD mechanism to exhibit the isochronal orientational cross-correlation under the shear. The β is plotted against the normalized shear rate $\dot{\gamma}\langle\tau_G\rangle_w$.

5.2.1. Orientation Distribution of Entanglement Segments. We consider freely jointed β entanglement segments having the bond vectors $\mathbf{u}_n = a\tilde{\mathbf{u}}_n$ ($|\tilde{\mathbf{u}}_n| = 1$; $n = 1, 2, ..., \beta$). This sequence of the segments, hereafter referred to as the subchain, takes various conformations under a given end-to-end vector $\mathbf{r}$ ($=\sum_{n=1}^{\beta} \mathbf{u}_n$); see Figure 16a.

As explained in Appendix A, we considered a symmetry of the conformation distribution of the subchain around its end-to-end axis to derive a relationship between the isochronal average of $\tilde{\mathbf{u}}\tilde{\mathbf{u}}$ and the normalized end-to-end vector $\tilde{\mathbf{r}} = \mathbf{r}/r$ ($r = |\mathbf{r}|$)

$$\langle\tilde{\mathbf{u}}\tilde{\mathbf{u}}\rangle_r = \langle\tilde{u}_r^2\rangle_r\,\tilde{\mathbf{r}}\tilde{\mathbf{r}} + \frac{1-\langle\tilde{u}_r^2\rangle_r}{2}[\mathbf{I} - \tilde{\mathbf{r}}\tilde{\mathbf{r}}] \qquad (21)$$

Here, $\mathbf{I}$ is the unit tensor, $\tilde{u}_r$ represents the component of $\tilde{\mathbf{u}}$ in the direction of $\tilde{\mathbf{r}}$ ($\tilde{u}_r = \tilde{\mathbf{u}}\cdot\tilde{\mathbf{r}}$), and $\langle\cdots\rangle_r$ denotes the conditional average under the *given* $\mathbf{r}$. The average $\langle\tilde{u}_r^2\rangle_r$ is a function of r and independent of $\tilde{\mathbf{r}}$. This $\langle\tilde{u}_r^2\rangle_r$ was calculated from a distribution function[38−40] of an end-to-end vector $\mathbf{r}'$ of a subsequence of $\beta - 1$ segments (cf. Figure 16b), as explained in Appendix B.

For several β values, Figure 17 shows plots of $\langle\tilde{u}_r^2\rangle_r$ against the reduced end-to-end distance of the subchain, $r/\beta a$ (βa = full-stretch length of the subchain). For small β values, the plot at $r/\beta a < 0.8$ changes with β. However, for larger β values, the plot becomes insensitive to β; see the plots for $\beta = 5$ and 8. (The plot was indistinguishable for $\beta = 8$ and $\beta \geq 9$.) More importantly, $\langle\tilde{u}_r^2\rangle_r$ for large $r/\beta a$ (> 0.8) is universally dependent on $r/\beta a$ irrespective of the β value.

The end-to-end vector $\mathbf{r}$ of the subchain has distributions in its orientation ($\tilde{\mathbf{r}}$) as well as length (r). Thus, the viscoelastically measured $\langle\tilde{\mathbf{u}}\tilde{\mathbf{u}}\rangle$ (cf. eqs 3−5) is obtained as an average of $\langle\tilde{\mathbf{u}}\tilde{\mathbf{u}}\rangle_r$ (eq 21) over these two distributions:

$$\langle\tilde{\mathbf{u}}\tilde{\mathbf{u}}\rangle = \overline{\langle\tilde{u}_r^2\rangle}\langle\tilde{\mathbf{r}}\tilde{\mathbf{r}}\rangle + \frac{1-\overline{\langle\tilde{u}_r^2\rangle}}{2}[\mathbf{I} - \langle\tilde{\mathbf{r}}\tilde{\mathbf{r}}\rangle] \qquad (22)$$

Here, $\overline{\langle\tilde{u}_r^2\rangle}$ is the average of $\langle\tilde{u}_r^2\rangle_r$ over the distribution of r (note that $\langle\tilde{u}_r^2\rangle_r$ depends only on r), and $\langle\tilde{\mathbf{r}}\tilde{\mathbf{r}}\rangle$ is the average of $\tilde{\mathbf{r}}\tilde{\mathbf{r}}$ over the orientational distribution.

At equilibrium, $\tilde{\mathbf{r}}$ is isotropically distributed to have $\langle\tilde{\mathbf{r}}\tilde{\mathbf{r}}\rangle = \mathbf{I}/3$, and eq 22 gives the well-known result, $\langle\tilde{\mathbf{u}}\tilde{\mathbf{u}}\rangle = \mathbf{I}/3$. However, under fast shear, $\tilde{\mathbf{r}}$ should be anisotropically distributed. For this case, eq 22 specifies a nontrivial relationship between $\langle\tilde{\mathbf{r}}\tilde{\mathbf{r}}\rangle$ and $\langle\tilde{\mathbf{u}}\tilde{\mathbf{u}}\rangle$.

5.2.2. CCR—DTD Relationship between $\langle\tilde{\mathbf{r}}\tilde{\mathbf{r}}\rangle$ and $\langle\tilde{\mathbf{u}}\tilde{\mathbf{u}}\rangle$. In the DTD molecular picture, the *internally equilibrated* subchains work as the independently stress-sustaining units.[3,18−20] Then, the deviatoric part of the stress tensor, unequivocally expressed in terms of $\tilde{\mathbf{u}}$ (cf. eq 1), is also written in terms of the end-to-end vector $\mathbf{r}$ of the subchain composed of β entanglement segments,

$$\boldsymbol{\sigma} = \frac{3\nu(N_{chain}/\beta)fk_BT}{\beta a^2}\left\{\langle\mathbf{rr}\rangle - \langle\mathbf{r}^2\rangle\frac{\mathbf{I}}{3}\right\} \qquad (23)$$

Here, the factor N_{chain}/β indicates the number of the subchains per chain, and βa^2 is the mean-square end-to-end distance of the subchain at equilibrium.

The shear-oriented entanglement segments in the subchain are not stretched but have the orientational cross-correlation. Because of this cross-correlation, the average end-to-end distance $\langle r^2\rangle^{1/2}$ of the subchain under the shear should be larger than the equilibrium average, $\langle r^2\rangle_{eq}^{1/2} = \beta^{1/2}a$: Considering this point, we introduce a stretch ratio λ_r for the subchain to rewrite eq 23 as

$$\boldsymbol{\sigma} = 3G_N\frac{\lambda_r^2}{\beta}\left\{\langle\tilde{\mathbf{r}}\tilde{\mathbf{r}}\rangle - \frac{\mathbf{I}}{3}\right\} \text{ with } \lambda_r^2 = \frac{\langle r^2\rangle}{\langle r^2\rangle_{eq}} \geq 1 \qquad (24)$$

Here, G_N ($=\nu N_{chain}fk_BT$) is the entanglement plateau modulus.

From eqs 1 and 24, we note that the $\langle\tilde{\mathbf{r}}\tilde{\mathbf{r}}\rangle$ of the subchain and the $\langle\tilde{\mathbf{u}}\tilde{\mathbf{u}}\rangle$ of the mutually equilibrated and orientationally correlated segments should satisfy a relationship

$$\frac{\lambda_r^2}{\beta}\left\{\langle\tilde{\mathbf{r}}\tilde{\mathbf{r}}\rangle - \frac{\mathbf{I}}{3}\right\} = \langle\tilde{\mathbf{u}}\tilde{\mathbf{u}}\rangle - \frac{\mathbf{I}}{3} \text{ for DTD} \qquad (25)$$

At $\dot{\gamma} \ll 1/\langle\tau_G\rangle_w$, the shear induces neither the orientational cross-correlation nor the subchain stretching, i.e., $\beta = \lambda_r = 1$. For this case, eq 25 gives a simple relationship for the TCR-induced DTD, $\langle\tilde{\mathbf{r}}\tilde{\mathbf{r}}\rangle = \langle\tilde{\mathbf{u}}\tilde{\mathbf{u}}\rangle = \mathbf{I}/3 + O(\dot{\gamma})$. However, under the fast shear, $\langle\tilde{\mathbf{r}}\tilde{\mathbf{r}}\rangle$ and $\langle\tilde{\mathbf{u}}\tilde{\mathbf{u}}\rangle$ should largely deviate from $\mathbf{I}/3$. Then, eq 25 provides us with a useful information about λ_r and β for the CCR−DTD process, as explained below.

For this process, we can equate the $\langle\tilde{\mathbf{u}}\tilde{\mathbf{u}}\rangle$ terms given by eqs 22 and 25 to find a relationship (under a condition that $\langle\tilde{\mathbf{r}}\tilde{\mathbf{r}}\rangle \neq \mathbf{I}/3$),

$$\overline{\langle\tilde{u}_r^2\rangle} = \frac{1}{3} + \frac{2\lambda_r^2}{3\beta} \text{ for CCR−DTD under fast shear} \qquad (26)$$

In addition to this CCR−DTD relationship between $\overline{\langle\tilde{u}_r^2\rangle}$ and λ_r^2/β, a general relationship is derived from the $r/\beta a$ dependence of $\langle\tilde{u}_r^2\rangle_r$ shown in Figure 17. Namely, $\overline{\langle\tilde{u}_r^2\rangle}$ is calculated as the average of $\langle\tilde{u}_r^2\rangle$ according to the distribution of r under the shear.

This distribution of r is not specified from our rheodielectric experiments. However, under the fast shear where eq 26 is valid, we expect that r is rather narrowly distributed. For this case, the variable utilized in Figure 17, $r/\beta a$, may be approximately replaced by $\langle r^2\rangle^{1/2}/\beta a = \lambda_r/\beta^{1/2}$ and the corresponding $\langle\tilde{u}_r^2\rangle_r$ may read as $\overline{\langle\tilde{u}_r^2\rangle}$. Under this approximation, eq 26 is shown in Figure 17

with the dotted curve. Requiring the general relationship explained above (plots in Figure 17) and eq 26 (dotted curve) to be satisfied simultaneously in the subchain-stretch regime $\lambda_r > 1$, we find

$$\lambda_r = \beta^{1/2} \quad \text{and} \quad \overline{\langle \tilde{u}_r^2 \rangle} = 1 \tag{27}$$

Equation 27 suggests that the subchain is fully stretched when the entanglement segments therein are mutually equilibrated through the CCR−DTD mechanism under the fast shear. These entanglement segments are not stretched but coherently orientated in the direction of **r**, thereby resulting in this full stretch of the subchain. For this case, we find the coincidence of the isochronal cross-correlation and auto-correlation, $\langle \tilde{\mathbf{u}}\tilde{\mathbf{u}}' \rangle = \langle \tilde{\mathbf{u}}\tilde{\mathbf{u}} \rangle$ $(=\langle \tilde{\mathbf{r}}\tilde{\mathbf{r}} \rangle)$, and the second-order moment averages appearing in eq 12 satisfy a CCR−DTD relationship,

$$\langle \tilde{u}_y \tilde{u}_y' \rangle = \langle \tilde{u}_y^2 \rangle \quad \text{under fast shear} \tag{28}$$

Concerning this result, we should emphasize that the strong orientational cross-correlation emerges only at the length scale of the bond vectors **u** of the entanglement segments. As schematically shown in Figure 18 (for the case of $\beta = 2$), many monomeric bond vectors (thin arrows) are included in each segment so that these vectors have a large freedom in their orientation. Because of this freedom, the distribution of the monomeric bond vectors *around* **u** (thick arrows) is negligibly affected by the shear, meaning that the isochronal orientational cross-correlation is vanishingly small at the length scale of the monomeric units even under the fast shear (as long as the entanglement segments are not stretched).

5.2.3. Shear Rate Dependence of β. Utilizing eq 28, we can rewrite eq 12 as $\Delta\epsilon(\dot{\gamma})/\Delta\epsilon(0) = 3\beta\langle \tilde{u}_y^2 \rangle$. Then, the number β of the entanglement segments exhibiting the isochronal orientational correlation can be evaluated as the ratio of the rheodielectric $\Delta\epsilon(\dot{\gamma})/\Delta\epsilon(0)$ data to the viscoelastic $3\langle \tilde{u}_y^2 \rangle$ data (cf. Figures 14 and 15). In Figure 19, the β thus obtained for the I-1190 and 6(I-179) chains are plotted against the normalized shear rate, $\dot{\gamma}\langle \tau_G \rangle_w$. (Under the slow shear at $\dot{\gamma} \leq 1/\langle \tau_G \rangle_w$, the approximation of narrowly distributed r utilized in derivation of eq 27 may be questionable. However, under such slow shear, the $\Delta\epsilon(\dot{\gamma})/\Delta\epsilon(0)$ and $\langle \tilde{u}_y^2 \rangle$ data are very close to 1 and $^1/_3$, respectively; see Figures 14 and 15. Thus, the $\{\Delta\epsilon(\dot{\gamma})/\Delta\epsilon(0)\}/3\langle \tilde{u}_y^2 \rangle$ ratio gives the correct β value (=1; for the case no CCR−DTD) also for $\dot{\gamma} \leq 1/\langle \tau_G \rangle_w$.)

As noted from Figure 19, the β for the linear I-1190 chain gradually increases to $\cong 1.8$ with increasing $\dot{\gamma}$ up to $30/\langle \tau_G \rangle_w$. The increase observed for the star 6(I-179) chain is less significant. This difference between the linear and star chains may be related to a difference in their TCR−DTD processes at equilibrium, as discussed below.

The β shown in Figure 19 is rheodielectrically obtained on the basis of the CCR−DTD picture and thus represents the number (β_{CCR}) of the segments that are mutually equilibrated and orientationally correlated due *only* to the CCR−DTD mechanism under the shear: This β_{CCR} is reduced to unity at equilibrium (for $\dot{\gamma} \to 0$). However, even at equilibrium, some number (β_{TCR}) of the segments are mutually equilibrated through the TCR−DTD mechanism,[12−17] although these segments are isotropically oriented to exhibit no isochronal orientational cross-correlation.[41] Thus, under the shear, the mutual equilibration would occur through both CCR−DTD and TCR−DTD processes (with the latter process resulting from *nonconvective* motion of the chain under the shear), and the net number β_s of the equilibrated segments is larger than β_{CCR}. We may utilize a DTD relationship between β and the dielectric Φ,[12,13,15] $\beta \cong \Phi^{-1}$, to estimate this β_s as

$$\beta_s \cong \beta_{CCR}\beta_{TCR} \tag{29}$$

Here, we have assumed that the CCR−DTD and TCR−DTD processes occur independently and the Φ_s $(\cong \beta_s^{-1})$ for the net DTD process is given by a product $\Phi_{CCR}\Phi_{TCR}$ $(\cong \beta_{CCR}^{-1}\beta_{TCR}^{-1})$.

The CCR is strongly enhanced with increasing shear rate, while the TCR would change with the shear rate just moderately. Thus, under sufficiently fast shear, the CCR would overwhelm the TCR to govern the β_s value. Since the CCR process is activated by the shrinkage of a transiently elongated chain and this shrinkage should be similar for the linear and star chains, these chains would have a similar β_s value under such fast shear. On the other hand, the β_{TCR} value at equilibrium is smaller for the linear chain than for the star chain,[14] and this would be the case also under the shear (because the shear would affect the TCR process just moderately). From these considerations, we naturally expect that the β_{CCR} is larger (i.e., the shear-induced orientational cross-correlation of the segments is more significant) for the linear chain; cf. eq 29. This expectation is in harmony with the β data $(=\beta_{CCR})$ shown in Figure 19.

Thus, the difference of the β of the linear and star chains appears to be essentially related to the difference in their TCR−DTD processes. However, we should emphasize that the above discussion is just qualitative, because the β_s and β_{TCR} values have not been quantitatively determined. In addition, the assumption of the independent CCR−DTD and TCR−DTD processes (underlying eq 29) may need to be modified in a quantitative discussion. Further experimental and theoretical studies are necessary for the difference of the CCR−DTD/TCR−DTD processes of the linear and star chains under the shear.

5.2.4. Additional Comment for β. The β $(=\beta_{CCR})$ was introduced in eq 9 as a cutoff distance for the isochronal cross-correlation of the segments. In other words, eq 9 considers that the correlation is locally concentrated. Consequently, the analysis on the basis of eq 9 gave the very strong correlation $(\langle \tilde{\mathbf{u}}\tilde{\mathbf{u}} \rangle = \langle \tilde{\mathbf{u}}\tilde{\mathbf{u}}' \rangle)$ that survives only for a short sequence ($\beta \leq 1.8$; see Figure 19). The full stretch of the subchain deduced from this analysis is a natural consequence of this treatment (localization) of the cross-correlation.

As the other choice, one may replace β in eq 9 by N_{chain} to define the orientational cross-correlation averaged over the chain contour (not over the β segments). The magnitude of the cross-correlation $\langle \tilde{\mathbf{u}}\tilde{\mathbf{u}}' \rangle$ obtained with this treatment is much smaller, by a factor of $O(\beta/N_{chain})$, than that resulting from the above analysis. However, with either treatments, the importance of the mutual equilibration (inducing the isochronal cross-correlation) is deduced from the difference between the $\Delta\epsilon(\dot{\gamma})/\Delta\epsilon(0)$ and $3\langle \tilde{u}_y^2 \rangle$ data (Figures 14 and 15).

5.2.5. Shear-Induced Acceleration of Dielectric Relaxation. The cross-correlation due to the CCR−DTD over the β segments (Figure 19) would reflect the increase of the equilibrated segment number (from β_{TCR}

to β_s) that is equivalent to an increase of an effective M_e by the factor of $\beta = \beta_s/\beta_{TCR}$. For both linear and star chains, this increase of M_e leads to the decrease of the stress (as represented by the N_{chain}/β factor in eq 23). However, the increase of M_e appears to have different effects on the dielectric relaxation rates of these chains, as discussed below.

Star Chain. For entangled star chains, the increase of M_e results in a decrease of the entropic penalty for the arm retraction.[19,20] For PI stars, the terminal dielectric relaxation at equilibrium is dominated by the TCR mechanism, but the rate-determining step for this TCR relaxation is the arm retraction over a certain contour length.[17] Thus, we naturally expect that the shear-induced increase of M_e (by a factor of β) accelerates the dielectric relaxation of the star chain.

On the basis of this argument, we may utilize an empirical equation for the $\langle\tau_\epsilon\rangle_{w,eq}$ data of entangled bulk PI at equilibrium,[16,17] $\langle\tau_\epsilon\rangle_{w,eq} \propto \exp\{\nu' M_a/M_e\}$ with $\nu' \cong 0.6$, to estimate the $\langle\tau_\epsilon\rangle_w$ under the steady shear as

$$\langle\tau_\epsilon\rangle_w = \langle\tau_\epsilon\rangle_{w,eq} \exp\left\{[\beta^{-1} - 1]\frac{0.6M_a}{M_e}\right\} \qquad (30)$$

(The M_e included in eq 30 represents the M_e at equilibrium.)

Utilizing the β data of the star PI chain (Figure 19) in eq 30, we estimated the $\langle\tau_\epsilon\rangle_w/\langle\tau_\epsilon\rangle_{w,eq}$ ratio. The results were consistent with the observed acceleration: For example, for the 20 and 25 wt % star PI chain at the largest $\dot\gamma$ examined, the estimated $\langle\tau_\epsilon\rangle_w/\langle\tau_\epsilon\rangle_{w,eq}$ ratio was 0.5 and 0.6, respectively, while the observed ratio was $\cong$ 0.4 and 0.7 (Figure 13). Thus, the observed acceleration of the dielectric relaxation is attributable to the increase of M_e reflecting the mutual equilibration of the segments due to the CCR−DTD mechanism under the shear.

Linear Chain. Now, we turn our attention to the linear chain. If we *assume* that the increase of M_e *always* accelerates the relaxation of linear chains, we expect a relationship $\langle\tau_\epsilon\rangle_w/\langle\tau_\epsilon\rangle_{w,eq} = \beta^{-1.5}$ (as suggested from an empirical equation,[15] $\langle\tau_\epsilon\rangle_{w,eq} \propto M^{3.5}/M_e^{1.5}$). However, the observed acceleration is much weaker than this expectation: For example, for the 15 wt % linear I-1190 chain under the fastest shear, the expected $\langle\tau_\epsilon\rangle_w/\langle\tau_\epsilon\rangle_{w,eq}$ ratio is $\cong$ 0.4 ($\beta \cong$ 1.8; cf. Figure 19) while the observed ratio is $\cong$0.9 (Figure 12). This disagreement between the expected and observed ratios indicates the invalidity of the above assumption. For further discussion of this point, the effect of M_e on the *linear* viscoelastic relaxation behavior is revisited below.

For blends of long and short chains having the molecular weights M_2 and M_1, an effective M_e for the long chain at long times increases on blending and the modulus decreases accordingly.[3] However, this increase of M_e does *not* always accelerate the linear viscoelastic relaxation of the long chain:[3,42,43] The acceleration is observed only when the Struglinski-Graessley parameter[43,44] $R_{SG} = M_2 M_e^2/M_1^3$ (with M_e being the entanglement spacing in the monodisperse systems) is larger than 0.1.[3]

In the tube model, this result is related to competition of the reptation along the dilated tube and the other type of reptation along the undilated tube moving (fluctuating) in a supertube:[44] The R_{SG} is proportional to a τ_{rep}/τ_{TCR} ratio, where $\tau_{rep} \propto M_2^3/M_e$ is the reptation time of the long chain in the moving/undilated tube and $\tau_{TCR} \propto \{M_2/M_e\}^2\{M_1^3/M_e\}$ is the time required for TCR throughout the long chain contour. The equilibration of the contour length *measured along the dilated tube*, a prerequisite for the reptation along this tube, requires a time $\sim\tau_{TCR}$.[3] Thus, this type of reptation overwhelms the reptation along the moving/undilated tube to accelerate the relaxation of the long chain only when τ_{TCR} is sufficiently smaller than τ_{rep} (i.e., for large R_{SG}).

Consequently, for small R_{SG}, the long chain reptates along the moving/undilated tube and the increase of the effective M_e does not accelerates the relaxation. In particular, this is the case for well entangled monodisperse systems (having $R_{SG} = M_e^2/M^2 \ll 1$).

The above argument does not include the contour length fluctuation (CLF) mechanism and is qualitative. However, that argument is still useful for our discussion of the rheodielectric $\langle\tau_\epsilon\rangle_w$ of the linear I-1190 chain. Namely, the $\langle\tau_\epsilon\rangle_w$ under the shear would be also determined by the competition of the reptation (with CLF) along the undilated/moving tube and the reptation along the dilated tube (both being affected by the CCR mechanism). The key motion in the CCR process for a given probe chain, the shrinkage of surrounding chains transiently stretched under the shear, would not lead to the full decay of the dielectric memory of the probe (as long as the subchain stretch specified by eq 27 occurs for the probe) but should accelerate the latter type of reptation of the probe (by effectively enlarging the tube for the probe).

The reptation along the undilated/moving tube governs the relaxation of monodisperse linear chains in the zero-shear limit.[3] Thus, the $\langle\tau_\epsilon\rangle_w$ under the shear should be close to the $\langle\tau_\epsilon\rangle_{w,eq}$ *if* the same type of reptation dominates the terminal chain motion under the shear. This seems to be the case for the I-1190 chain at the shear rates examined, as judged from the weak $\dot\gamma$ dependence of $\langle\tau_\epsilon\rangle_w$ (Figure 12). Of course, this argument does not rule out a possibility that the other type of reptation along the dilated tube becomes dominant at higher rates to significantly decrease $\langle\tau_\epsilon\rangle_w$.

The time required for the equilibration of the chain contour length measured along the dilated tube is a key for a more detailed discussion of the $\langle\tau_\epsilon\rangle_w$ under the shear: A ratio of this time and the reptation time in the undilated/moving tube would determine the competition of the two types of reptation, as similar to the situation in the linear viscoelastic regime. However, the length equilibration time under the shear would be affected by CCR and not necessarily identical to the τ_{TCR} at equilibrium, and further theoretical studies of this time are necessary for the detailed discussion of $\langle\tau_\epsilon\rangle_w$.

5.2.6. Comment for the CCR Model for Linear Chain. Finally, we make a brief comment for the current CCR models developed for linear chains.[8−10] In these models, the relaxation time $\tau_G(\dot\gamma)$ defined for $\langle\mathbf{uu}\rangle$ decreases under the shear because of the CCR mechanism. The magnitude of this decrease is essentially determined by a factor $F_{CCR} = \dot\gamma\sigma_s\tau_G(0)/G_N$, where σ_s and $\tau_G(0)$ are the shear stress under the flow and the linear viscoelastic relaxation time, respectively. At the largest $\dot\gamma$ examined in this study, the F_{CCR} factor for the I-1190 chain increases up to $\cong$ 10 and the $\tau_G(\dot\gamma)$ calculated from the models exhibits an order of magnitude decrease, $\tau_G(\dot\gamma)/\tau_G(0) \sim O(10^{-1})$.

This decrease of $\tau_G(\dot\gamma)$ is much more significant than the decrease observed for the dielectric $\langle\tau_\epsilon\rangle_w$ of the linear I-1190 chain (Figure 12). Of course, the current CCR

models are formulated for the isochronal $\langle \mathbf{uu} \rangle$, and $\tau_G(\dot{\gamma})$ specifying the relaxation of $\langle \mathbf{uu} \rangle$ is different from the dielectric $\langle \tau_\epsilon \rangle_w$ characterizing the decay of the cross-correlation $\langle \tilde{u}_y(n,t+t_r)\tilde{u}_y(n',t_r) \rangle$ at two separate times $t + t_r$ and t_r (cf. eq 8). However, if we extend these models to the dielectric properties in the simplest way,[45] the decrease of $\langle \tau_\epsilon \rangle_w$ under the shear appears to be essentially the same as the large decrease of $\tau_G(\dot{\gamma})$ explained above. Thus, this extension requires a detailed consideration of the terminal motion of the chain under the flow. This motion deserves further theoretical studies.

6. Concluding Remarks

For entangled solutions of linear and star *cis*-polyisoprene (PI) chains having the type-A dipoles parallel along the chain backbone, we have examined the rheodielectric behavior under the steady shear. This behavior was detected in the shear-gradient direction. At the shear rates $\dot{\gamma}$ examined, the chains were not stretched but orientated in the shear direction.

For the linear chain, the dielectric intensity $\Delta\epsilon$ and relaxation time $\langle \tau_\epsilon \rangle_w$ decreased only slightly (by a factor of $\cong$ 10%) with increasing $\dot{\gamma}$ up to $30/\langle \tau_G \rangle_w$. The star chains exhibited more prominent decreases of $\Delta\epsilon$ and $\langle \tau_\epsilon \rangle_w$. However, for both chains, the decreases of $\Delta\epsilon$ and $\langle \tau_\epsilon \rangle_w$ were much less significant compared to the order of magnitude decreases of the viscosity η and the first normal stress coefficient Ψ_1. These rheodielectric and viscoelastic data were analyzed to reveal some characteristic features of the chain conformation and dynamics under the steady shear.

The $\Delta\epsilon$ reflects the chain dimension $\langle R_y^2 \rangle$ in the shear gradient direction (y direction). Comparing the $\Delta\epsilon$ data with the viscoelastically evaluated $\langle \tilde{u}_y^2 \rangle$ of the entanglement segments, we found a strong isochronal orientational cross-correlation of these segments under fast shear.

This cross-correlation was related to the dynamic tube dilation (DTD) induced by the convective constraint release (CCR) under the shear: With this CCR−DTD mechanism, some number (β) of segments are mutually equilibrated to exhibit the isochronal cross-correlation. On the basis of this CCR−DTD molecular picture, the $\Delta\epsilon$ data were further analyzed to separately evaluate the number β and the magnitude of cross-correlation $\langle \tilde{u}_y \tilde{u}_y' \rangle$. It turned out that β increases up to $\cong$1.8 and $\cong$1.2 for the linear and star chains with increasing $\dot{\gamma}$ up to $30/\langle \tau_G \rangle_w - 40/\langle \tau_G \rangle$, respectively, and $\langle \tilde{u}_y \tilde{u}_y' \rangle$ under high shear coincides with $\langle \tilde{u}_y^2 \rangle$. The weak $\dot{\gamma}$ dependence of the $\Delta\epsilon$ data, reflecting the strong cross-correlation characterized with these β and $\langle \tilde{u}_y \tilde{u}_y' \rangle$, demonstrates the importance of the CCR−DTD mechanism.

The $\langle \tau_\epsilon \rangle_w$ specifies the rate of conformational fluctuation in the shear gradient direction. For the star chain, the observed decrease of $\langle \tau_\epsilon \rangle_w$ (by a factor of $\cong$ 40% at the largest $\dot{\gamma}$) was related to a small increase of an effective M_e resulting from the mutual equilibration due to the CCR mechanisms. In fact, a decrease of $\langle \tau_\epsilon \rangle_w$ estimated from this increase of M_e (by the above β value) was in close agreement with the observed decrease.

In contrast, for the linear chain, a decrease of $\langle \tau_\epsilon \rangle_w$ similarly estimated from the increase of M_e was much more significant than the observation. This result was related to the competition of the reptation along the undilated/moving tube and the other type of the reptation along the dilated tube. In the range of $\dot{\gamma}$ examined, the former type of reptation appears to dominate the terminal relaxation thereby giving the $\dot{\gamma}$ -insensitive $\langle \tau_\epsilon \rangle_w$.

Finally, the weak $\dot{\gamma}$ dependence of $\langle \tau_\epsilon \rangle_w$ of the linear chain is not straightforwardly deduced from the current CCR models. Further theoretical studies are desirable for this behavior of $\langle \tau_\epsilon \rangle_w$.

Acknowledgment. This work was supported by the Ministry of Education, Culture, Sports, Science, and Technology, Japan (Grant No. 12650884) and by Japan Chemical Innovation Institute (through the Doi Project). Y.M. acknowledges, with thanks, financial support from the JSPS Research Fellowship for Young Scientist.

Appendix A. Dyadic $\langle \mathbf{u\tilde{u}} \rangle$ of Mutually Equilibrated Entanglement Segments

We consider the freely jointed β entanglement segments (cf. Figure 16a). The sequence of these segments (subchain) are equilibrated under a *given* end-to-end vector $\mathbf{r}$ ($=a\sum_{n=1}^{\beta} \tilde{\mathbf{u}}_n$), where $\tilde{\mathbf{u}}_n$ is the unit bond vector of the nth segment. For the formulation of the dyadic $\langle \tilde{\mathbf{u}}\tilde{\mathbf{u}} \rangle$, we introduce a Cartesian coordinates X, Y, and Z with the Z axis being parallel to $\mathbf{r}$; see Figure 16b. The components of $\tilde{\mathbf{u}}_n$ in this XYZ-coordinate system are denoted by $\tilde{u}_{n,X}$, $\tilde{u}_{n,Y}$, $\tilde{u}_{n,r}$.

The isochronal cross-correlation of these components vanishes because the conformation of the subchain is symmetrically distributed around the Z axis. Thus, in the XYZ-coordinate system, the isochronal average of $\tilde{\mathbf{u}}\tilde{\mathbf{u}}$ over the β segments can be expressed in a diagonalized form,

$$<\tilde{\mathbf{u}}\tilde{\mathbf{u}}>_r = \begin{bmatrix} \langle \tilde{u}_\rho^2 \rangle_r & 0 & 0 \\ 0 & \langle \tilde{u}_\rho^2 \rangle_r & 0 \\ 0 & 0 & \langle \tilde{u}_r^2 \rangle_r \end{bmatrix} \qquad \text{(A1)}$$

with

$$\langle \tilde{u}_r^2 \rangle_r = \frac{1}{\beta}\sum_{n=1}^{\beta} \tilde{u}_{n,r}^2 \quad \text{and} \quad \langle \tilde{u}_\rho^2 \rangle_r = \frac{1}{2}(1 - \langle \tilde{u}_r^2 \rangle_r) \qquad \text{(A2)}$$

Here, $\langle \cdots \rangle_r$ represents the conditional average under the *given* $\mathbf{r}$. The $\langle \tilde{u}_r^2 \rangle_r$ given by eq A2 is a function of $r = |\mathbf{r}|$ and independent of the subchain orientation specified by the normalized end-to-end vector, $\tilde{\mathbf{r}} = \mathbf{r}/r$. The explicit calculation of $\langle \tilde{u}_r^2 \rangle_r$ is made in Appendix B.

Now, we return to the experimental xyz-coordinate system with the x and y directions being chosen as the shear and shear-gradient directions (Figure 16a). Transforming the diagonal expression (eq A1) into this coordinate system, we obtain a general tensorial expression of $\langle \tilde{\mathbf{u}}\tilde{\mathbf{u}} \rangle_r$,

$$\langle \tilde{\mathbf{u}}\tilde{\mathbf{u}} \rangle_r = \langle \tilde{u}_r^2 \rangle_r \tilde{\mathbf{r}}\tilde{\mathbf{r}} + \frac{1 - \langle \tilde{u}_r^2 \rangle_r}{2}[\mathbf{I} - \tilde{\mathbf{r}}\tilde{\mathbf{r}}] \qquad \text{(A3)}$$

The subchain has distributions in its orientation and length. Thus, $\langle \tilde{\mathbf{u}}\tilde{\mathbf{u}} \rangle$ of the segment (determining the viscoelastic stress) is obtained as the average of $\langle \tilde{\mathbf{u}}\tilde{\mathbf{u}} \rangle_r$ over these two distributions (cf. eq 22).

Appendix B. Evaluation of $\langle \tilde{u}_r^2 \rangle_r$

For the subchain composed of freely jointed β segments (Figure 16), the component of the bond vector $\tilde{u}_r$

($=\tilde{\mathbf{r}}\cdot\tilde{\mathbf{u}}$) exhibits a distribution under a constraint $\mathbf{r} = a\sum_{n=1}^{\beta}\tilde{\mathbf{u}}_n$. The average $\langle\tilde{u}_r{}^2\rangle_r$ under a given $\mathbf{r}$ (defined by eq A2) can be calculated in the following way.

For $\beta = 2$. In the subchain composed of two segments, $\tilde{u}_r$ and r are perfectly correlated unless $r = 0$; $\tilde{u}_r = r/2a$ for $0 < r \le 2a$. For $r = 0$, $\tilde{u}_r$ takes isotropic configuration. Thus, $\langle\tilde{u}_r{}^2\rangle_r$ is given by

$$\langle\tilde{u}_r{}^2\rangle_r = {}^1/_3 \quad \text{for } r/a = 0, \quad \langle\tilde{u}_r{}^2\rangle_r = r^2/4a^2 \quad \text{for } 0 < r/a \le 2 \tag{B1}$$

For $\beta \ge 3$. In the calculation of $\langle\tilde{u}_r{}^2\rangle_r$ for $\beta \ge 3$, we focus on a representative segment and utilize the distribution function $W(\mathbf{r}')$ of the end-to-end vector $\mathbf{r}'$ for a subsequence of the remaining $\beta - 1$ segments; see Figure 16b. Since all β segments are equivalent to each other, we can choose the first segment ($n = 1$) as the representative segment without losing the generality.

The *unnormalized* distribution function of $\mathbf{r}'$ is given by[38−40]

$$W(\mathbf{r}') = \frac{1}{\xi}\sum_{k=0}^{k\le(\beta-1-\xi)/2}\frac{(-1)^k(\beta-1)!}{k!(\beta-1-k)!}(\beta-1-2k-\xi)^{\beta-3} \tag{B2}$$

with

$$\xi = \frac{|r'|}{a} = \left\{\left(\frac{r}{a}\right)^2 + 1 - \left(\frac{2r}{a}\right)\cos\theta\right\}^{1/2} \quad (0 \le \xi \le \beta - 1) \tag{B3}$$

Here, θ is the polar angle of $\tilde{\mathbf{u}}$ defined with respect to $\mathbf{r}$ ($\tilde{u}_r = \cos\theta$); see Figure 16b. Thus, the average $\langle\tilde{u}_r{}^2\rangle_r$ is given by an integral

$$\langle\tilde{u}_r{}^2\rangle_r = \frac{\int_0^{\theta^*}\cos^2\theta\, W(\mathbf{r}'(\theta))\sin\theta\, d\theta}{\int_0^{\theta^*} W(\mathbf{r}'(\theta))\sin\theta\, d\theta} \tag{B4}$$

where the upper bound of this integral θ^* depends on the r/a value:

$$\theta^* = \pi \quad \text{for} \quad 0 \le r/a \le \beta\text{-}2,$$
$$\theta^* = \cos^{-1}\left\{\frac{(r/a)^2 + 1 - (\beta-1)^2}{2(r/a)}\right\} \quad \text{for } \beta - 2 < r/a \le \beta \tag{B5}$$

This dependence reflects a limitation of the ξ value ($\xi \le \beta - 1$): For $\beta - 2 < r/a \le \beta$, θ^* is smaller than π because the antiparallel configuration of $\mathbf{r}$ and $\tilde{\mathbf{u}}$ ($\theta = \pi$) gives $\xi > \beta - 1$ and is prohibited.

References and Notes

(1) Ferry, J. D. *Viscoelastic Properties of Polymers*, 3rd ed; Wiley: New York, 1980.
(2) Graessley, W. W. *Adv. Polym. Sci.* **1974**, *16*, 1.
(3) Watanabe, H. *Prog. Polym. Sci.* **1999**, *24*, 1253.
(4) Doi, M.; Edwards, S. F. *The Theory of Polymer Dynamics*; Clarendon: Oxford, England, 1986.
(5) Pearson, D. S.; Kiss, A. D.; Fetters, L. J.; Doi, M. *J. Rheol.* **1989**, *33*, 517.
(6) Pearson, D. S.; Herbolzheimer, E.; Grizzuti, N.; Marrucci, G. *J. Polym. Sci., Part B: Polym. Phys.* **1991**, *29*, 1589.
(7) Marrucci, G. *J. Non-Newtonian Fluid Mech.* **1996**, *62*, 279.
(8) Ianniruberto, G.; Marrucci, G. *J. Non-Newtonian Fluid Mech.* **1996**, *65*, 241.
(9) Mead, D. W.; Larson, R. G.; Doi, M. *Macromolecules* **1998**, *31*, 7895.
(10) Milner, S. T.; McLeish, T. C. B.; Likhtman, A. E. *J. Rheol.* **2001**, *45*, 539.
(11) Stockmayer, W. H. *Pure Appl. Chem.* **1967**, *15*, 539.
(12) Watanabe, H.; Matsumiya, Y.; Osaki, K. *J. Polym. Sci., B: Polym. Phys.* **2000**, *38*, 1024.
(13) Matsumiya, Y.; Watanabe, H.; Osaki, K. *Macromolecules* **2000**, *33*, 499.
(14) Matsumiya, Y.; Watanabe, H. *Macromolecules* **2001**, *34*, 5702.
(15) Watanabe, H. *Macromol. Rapid Commun.* **2001**, *22*, 127.
(16) Watanabe, H. *Korea-Aust. Rheol. J.* **2001**, *13*, 205.
(17) Watanabe, H.; Matsumiya, Y.; Inoue, T. *Macromolecules* **2002**, *35*, 2339.
(18) Marrucci, G. *J. Polym. Sci., Polym. Phys. Ed.* **1985**, *23*, 159.
(19) Ball, R. C.; McLeish, T. C. B. *Macromolecules* **1989**, *22*, 1911.
(20) Milner, S. T.; McLeish, T. C. B. *Macromolecules* **1997**, *30*, 2159; *ibid.* **1998**, *31*, 7479.
(21) Cole, R. H. *J. Chem. Phys.* **1965**, *42*, 637.
(22) Riande, E.; Saiz, E. *Dipole Moments and Birefringence of Polymers*; Prentice Hall: Englewood Cliffs, NJ, 1992.
(23) For isotropic materials in the stationary state, $\Theta(t)$ is reduced to the auto-correlation of the vectorial polarization $\mathbf{P}$; $\Theta(t) = \langle\mathbf{P}(t+t_r)\cdot\mathbf{P}(t_r)\rangle/3$.
(24) For a given segmental bond vector $\tilde{\mathbf{u}}$ of a particular chain, the bond vector of the other chain takes two opposite configurations ($\tilde{\mathbf{u}}_o$ and $-\tilde{\mathbf{u}}_o$) with the same probability either at equilibrium or under steady shear. Thus, the interchain cross-correlation $\langle\tilde{\mathbf{u}}\tilde{\mathbf{u}}_o\rangle$ does not contribute to $\Delta\epsilon$ and $\Phi(t)$.
(25) Watanabe, H.; Urakawa, O.; Kotaka, T. *Macromolecules* **1993**, *26*, 5073.
(26) Watanabe, H.; Sato, T.; Osaki, K. *Macromolecules* **1996**, *29*, 104.
(27) Hayakawa, R.; Kanda, H.; Sakamoto, M.; Wada, Y. *Jpn. J. Appl. Phys.* **1975**, *14*, 2039.
(28) Adachi, K.; Hirano, H. *Macromolecules* **1998**, *31*, 3958.
(29) Sato, T.; Watanabe, H.; Osaki, K. *Macromolecules* **1996**, *29*, 6231.
(30) Matsumiya, Y.; Watanabe, H.; Inoue, T.; Osaki, K.; Yao, M. L. *Macromolecules* **1998**, *31*, 7973.
(31) Milner, S. T.; McLeish, T. C. B. *Phys. Rev. Lett.* **1998**, *81*, 725.
(32) Takahashi, M.; Masuda, T.; Bessho, N.; Osaki, K. *J. Rheol.* **1980**, *24*, 517.
(33) Osaki, K.; Kimura, S.; Kurata, M. *J. Polym. Sci., Polym. Phys. Ed.* **1981**, *19*, 517.
(34) Magda, J. J.; Lee, C. S.; Muller, S. J.; Larson, R. G. *Macromolecules* **1993**, *26*, 1696.
(35) Brown, E. F.; Burghardt, W. R.; Kahvand, H.; Venerus, D. C. *Rheol. Acta* **1995**, *34*, 221.
(36) At T_r for the rheodielectric measurements, the local motion of monomeric segments of the PI chains was too fast to be detected in our experimental window shown in Figures 8−11.
(37) Muller, R.; Pesce, J. J.; Picot, C. *Macromolecules* **1993**, *26*, 4356.
(38) Nagai, K. *J. Phys. Soc. Jpn.* **1958**, *13*, 928.
(39) Hsiung, C.; Hsiung, H.; Gordus, A. *J. Chem. Phys.* **1964**, *34*, 535.
(40) Yamakawa, H. *Modern Theories of Polymer Solutions*; Harper & Row: New York, 1971.
(41) At equilibrium, the end-to-end vector of the subchain composed of β entanglement segments, $\mathbf{r} = \sum_{n=1}^{\beta}\mathbf{u}_n$, has a distribution characterized by $\langle\mathbf{rr}\rangle_{eq} = \beta a^2\mathbf{I}/3$. This $\langle\mathbf{rr}\rangle_{eq}$ coincides with a sum $\beta\langle\mathbf{uu}\rangle_{eq} + \beta(\beta-1)\langle\mathbf{uu}'\rangle_{eq}$. Since $\langle\mathbf{uu}\rangle_{eq} = a^2\mathbf{I}/3$, those segments have no isochronal cross-correlation at equilibrium ($\langle\mathbf{uu}'\rangle_{eq} = \mathbf{0}$).
(42) Watanabe, H.; Kotaka, T. *Macromolecules* **1984**, *17*, 2316.
(43) Struglinski, M. J.; Graessley, W. W. *Macromolecules* **1985**, *18*, 2630.
(44) Viovy, J. L.; Rubinstein, M.; Colby, R. H. *Macromolecules* **1991**, *24*, 3587.
(45) For example, the simplest extension of the Milner−McLeish−Likhtman model[10] can be made in the following way. In this model, the time evolution equation is formulated for the isochronal orientation function $\langle\mathbf{u}(s,t)\mathbf{u}(s',t)\rangle$ (with s and s' being the contour variables corresponding to n and n' utilized in this study). The cross-correlation function $\langle\mathbf{u}(s,t)\cdot\mathbf{u}(s',0)\rangle$ can be calculated from the same time evolution equation except that the operations with respect to s', included in the original equation,[10] are quenched.

MA020562Y